



Stratigraphy of the

# BURIED TEAYS VALLEY IN WESTERN OHIO AND EASTERN INDIANA

by Tyler A. Norris, T. Andrew Nash, Henry M. Loope, and José Luis Antinao



OPEN-FILE REPORT

**2022-2**

Columbus 2022



**DISCLAIMER:** The information contained herein has not been reviewed for technical accuracy and conformity with current ODNR Division of Geological Survey standards for published or open-file materials. The ODNR Division of Geological Survey does not guarantee this information to be free from errors, omissions, or inaccuracies and disclaims any responsibility or liability for interpretations or decisions based thereon.

**GRAPHIC DESIGN & LAYOUT:** Jeremy E. Gladden

**EDITING:** Anthony J. Bresnen

**FRONT COVER:** Rotary sonic drill rig setup (Frontz Drilling) at the site of Willshire-21 boring in Willshire, Ohio.

**RECOMMENDED CITATION:** Norris, T.A., Nash, T.A., Loope, H.M., and Antinao, J.L., 2022, Stratigraphy of the buried Teays Valley in western Ohio and eastern Indiana: Columbus, Ohio Department of Natural Resources, Division of Geological Survey Open-File Report 2022-2, 20 p.

## CONTENTS

Abstract.....	1
Introduction.....	1
Previous work.....	1
Project purpose.....	3
Methods.....	4
Drilling and core handling.....	4
Portable X-Ray Fluorescence (pXRF).....	5
Particle Size Analysis (PSA).....	5
Results.....	6
Core stratigraphy.....	6
Willshire-21 core stratigraphy.....	6
Domestic core stratigraphy.....	8
pXRF Results.....	9
PSA Results.....	10
Discussion.....	12
Conclusions and future work.....	12
Acknowledgments.....	12
References.....	15

## FIGURES

1. Location map of borings drilled in Ohio and Indiana.....	3
2. Diagram of the roto sonic drilling process.....	4
3. Willshire-21 stratigraphic column with selected results.....	7
4. Domestic stratigraphic column with selected results.....	8
5. Elements categorized by pXRF analysis on a periodic table.....	10
6. Grain size texture ternary plot and values for diamicton units.....	11
7. Cross section of Willshire-21 with bedrock surface models.....	13
8. Cross section of Domestic with bedrock surface models.....	14
A1-1. Willshire-21 pXRF plot of selected elements.....	17
A1-2. Domestic pXRF plot of selected elements.....	18

## TABLES

A1-1. Willshire-21 pXRF table.....	17
A1-2. Domestic pXRF table.....	18
A2-1. Willshire-21 PSA table.....	19
A2-2. Domestic PSA table.....	20

## APPENDICES

Appendix 1. pXRF data.....	17
Appendix 2. PSA data.....	19

## DATASETS

1. Dataset 1. Willshire-21 core photographs.....	web link
2. Dataset 2. Domestic core photographs.....	web link
3. Dataset 3. Willshire-21 core descriptions.....	web link
4. Dataset 4. Domestic core descriptions.....	web link

## ABBREVIATIONS USED IN THIS REPORT

degrees Celsius.....	C°	meters .....	m
degrees Fahrenheit .....	F°	millimeter .....	mm
feet .....	ft	optically stimulated luminesce.....	OSL
grams .....	g	particle size analysis.....	PSA
high density polyethylene.....	HDPE	parts-per-million.....	ppm
inductively coupled plasma		polyvinyl chloride .....	PVC
mass spectrometry.....	ICP-MS	portable X-ray fluorescence .....	pXRF
level of detection .....	LOD	X-ray diffraction .....	XRD
liter .....	L	X-ray fluorescence .....	XRF
mean sea level .....	m.s.l.		

# Stratigraphy of the Buried Teays Valley in western Ohio and eastern Indiana

by  
Tyler A. Norris<sup>1</sup>, T. Andrew Nash<sup>1</sup>,  
Henry M. Loope<sup>2</sup>, and José Luis Antinao<sup>2</sup>

## ABSTRACT

The Ohio Department of Natural Resources, Division of Geological Survey and Indiana Geological and Water Survey have characterized a regional section of the buried Teays-Mahomet (Teays) River Valley system through rotary sonic drilling. The Teays River, once part of a major pre-Quaternary drainage system, was altered and filled with unconsolidated deposits from multiple glacial events. Previous regional mapping efforts in the Teays Valley were limited by the complex and spatially variable nature of the valley's fill, as well as the uncertainty of the valley's local morphology. Passive seismic geophysical methods and pre-existing well log data first were used to locate ideal drilling locations within the buried valley in western Ohio and eastern Indiana. Two continuous cores were drilled through the Teays to allow for detailed description of the valley fill stratigraphy and subsampling for physical and geochemical analyses. This report describes the results of the drilling process and subsequent laboratory analyses.

## INTRODUCTION

The Teays River System was a major pre-Quaternary Period drainage network with a general flow from the southeast towards the northwest. This system transported surface water from the southern Appalachian Mountains across the lower Great Lakes Region and eventually met with the ancestral Mississippi River in central Illinois (Goldthwait, 1991). This drainage network was likely millions of years old prior to glaciation, developing as a result of uplift along the east coast of North America during the Appalachian Orogeny. This drainage network incised through the Paleozoic bedrock deposited in the Appalachian and Illinois Basins, creating an extensive valley with a main trunk about 1,000 miles long. Multiple glaciations occurred during the Quaternary Period that entirely buried large portions of this paleo drainage network in the lower Great Lakes region and altered the courses of many modern rivers outside of the glaciated area (Teller and Goldthwait, 1991). The modern, buried Teays River Valley contains a complex fill of unconsolidated clay, silt, sand, gravel, and diamicton deposits that vary regionally (Bleuer, 1991). Few studies have managed to effectively characterize the stratigraphy of the Quaternary-aged sediments within the Teays system.

## Previous Work

Some of the earliest research on the then-unnamed buried Teays Valley occurred in western Ohio and eastern Indiana. Bownocker (1899) examined the depth to bedrock in the glaciated region near the Ohio-Indiana border and identified the preglacial channel, but he did not study the sediments that filled the preglacial valley. In unglaciated southern Ohio, research detailing terraces, straths, and valley-fill sediments related to the preglacial drainage network originated with Tight (1903). Tight described drainage modifications and lacustrine terrace relationships in southern Ohio and surrounding regions and named the Teays Valley. Later while detailing the effects of glaciation on vegetation in southern Ohio, Wolfe (1942) described the series of events that led to the damming of the Teays River drainage network and

---

<sup>1</sup> Ohio Department of Natural Resources, Division of Geological Survey, 2045 Morse Rd. Bldg. B-2, Columbus, Ohio 43229

<sup>2</sup> Indiana Geological & Water Survey, 1001 E. 10th St., Bloomington, IN 47405

the formation of Lake Tight, which resulted in valley filling and terrace carving during a pre-Illinoian glaciation. Work since then has attempted to further define Lake Tight water levels and spatial extent (e.g., Erjavec, 2018).

Many previous studies built upon the drainage history and additional research across the lower Great Lakes region to define further the preglacial drainage network. Stout and others (1943) produced the first published map of the Teays River Valley and preglacial drainage networks for all of Ohio. Horberg's (1945) research connecting the Teays Valley of Ohio with the Mahomet Valley of Illinois completed the regional synthesis of preglacial drainage networks for early twentieth century research and created the modern conceptual understanding of the Teays-Mahomet drainage network. A variety of hypothesized drainage routes across Indiana to connect the Teays and Mahomet Valleys had been proposed by the time detailed bedrock topography mapping was completed for the glaciated portion of the state (Wayne, 1956; Gray, 1982).

Research in the unglaciated portion of Ohio provides sedimentological evidence for Lake Tight. Hoyer (1976) described deposits of exposed sections of the Parker Strath in southern Ohio, which Hoyer interpreted as basal alluvial sediments deposited prior to glaciation, and finer-grained Pleistocene-aged silt and clay lacustrine material (known as Minford Silt or Minford Clay) that accumulated within filled valleys during ice damming. The age of these sediments was further defined from paleomagnetic data in Jacobson and others (1988) and Bonnett and others (1991), revealing that ice damming of the Teays and its former tributaries occurred multiple times, creating several well-defined terrace elevations. While these studies provide insight into the drainage history and early Quaternary chronology of the Teays River Valley, they do not explain the glacial processes, nor the timing of those processes, that ultimately buried the valley in west-central Ohio and east-central Indiana.

The first significant subsurface investigation of the buried Teays Valley in central Ohio occurred in Madison, Clark, and Champaign Counties (Norris and Spicer, 1958). Boreholes were drilled within the deepest sections of the buried valley following results of geophysical resistivity surveys. Norris and Spicer discovered that in central Ohio, the lowermost deposits within the buried Teays Valley are often ice-dammed lake sediments and typically contain clay, silt, and fine sand. These fine-grained deposits are similar to the Minford Silt deposits found exposed at the surface in southern Ohio but here are overlain by Illinoian- and Wisconsinan-aged glacial tills and outwash (Norris and Spicer, 1958). Norris and Spicer (1958) correlated their basal lake sediments in central Ohio to the Minford Silt of southeast Ohio on the basis of physical characteristics and a maximum elevation of both units at 262 meters (m), or 860 feet (ft), above mean sea level (Tight, 1903; Wolfe, 1942). At its thickest, the Minford Silt is 80.5 m (264 ft) thick at the London Prison Farm in Madison County (Norris and Spicer, 1958). The interpretation of these sediments recovered from test hole borings provided the first strong evidence for the processes that buried the Teays River in Ohio. According to Norris and Spicer (1958), these thick Minford Silt deposits support the hypothesis that ice dammed the river during a pre-Illinoian glaciation near the northernmost reach of the ancient Teays River Valley, probably southwest of Fort Wayne, Indiana. Unfortunately, these boreholes were drilled with rotary drilling methods that did not preserve sediment cores for future analyses to further corroborate these claims. Norris and Spicer's (1958) research in central Ohio partly motivated further study of the valley-fill sediments farther down valley into Indiana.

In Indiana, the first large-scale effort to classify Quaternary-aged, Teays Valley fill through rotary drilling and gamma-ray logging began in 1977 (Bleuer, 1991). Bleuer (1991) synthesizes more than a decade's worth of drilling and gamma-ray logging data to present a comprehensive analysis of the glacial processes and sediments which fill bedrock valleys (Lafayette Bedrock Valley System) in northern Indiana. Included within this analysis is the presentation of a stratigraphic framework that combines mineralogical data and physical properties to classify units from Superior and Grenville provinces down to the member level. These units are correlated across Indiana and into Ohio through comparative analysis of gamma-ray logs collected at wells where samples were not available. Bleuer (1991) interpreted the sequences of sediments that filled the Lafayette Bedrock Valley System and theorized that nine major drainage stages existed within the Lafayette Bedrock Valley System between the onset of

the drainage network and through the Quaternary Period. While this existing stratigraphic framework provides evidence for the sequence of glacial events and processes that buried the Lafayette and Teays systems, there is almost no absolute age control on the sediments that infill these bedrock valleys.

### Project Purpose

In this report, we present the first detailed stratigraphic descriptions of the Quaternary-aged sediments that filled the Teays Valley in west-central Ohio and east-central Indiana. Two new rotary sonic cores were collected near Willshire, Ohio (Mercer County) and Domestic, Indiana (Jay County; fig. 1). The Willshire-21 core was collected at 40.691788, -84.773658 from February 23 to February 26, 2021. The Domestic core was collected at 40.546530, -85.079176 from March 2 to March 8, 2021. The stratigraphic descriptions of these cores are supported with geochemical data from portable x-ray fluorescence (pXRF) and particle size analysis (PSA) data through laser diffraction and sieving. Results from these analyses are structured to provide all the raw data collected during this study and to support future research on the Teays Valley in Ohio and Indiana. A brief discussion of how these new cores fit into the historical narrative of the Teays bedrock valley systems follows these results.

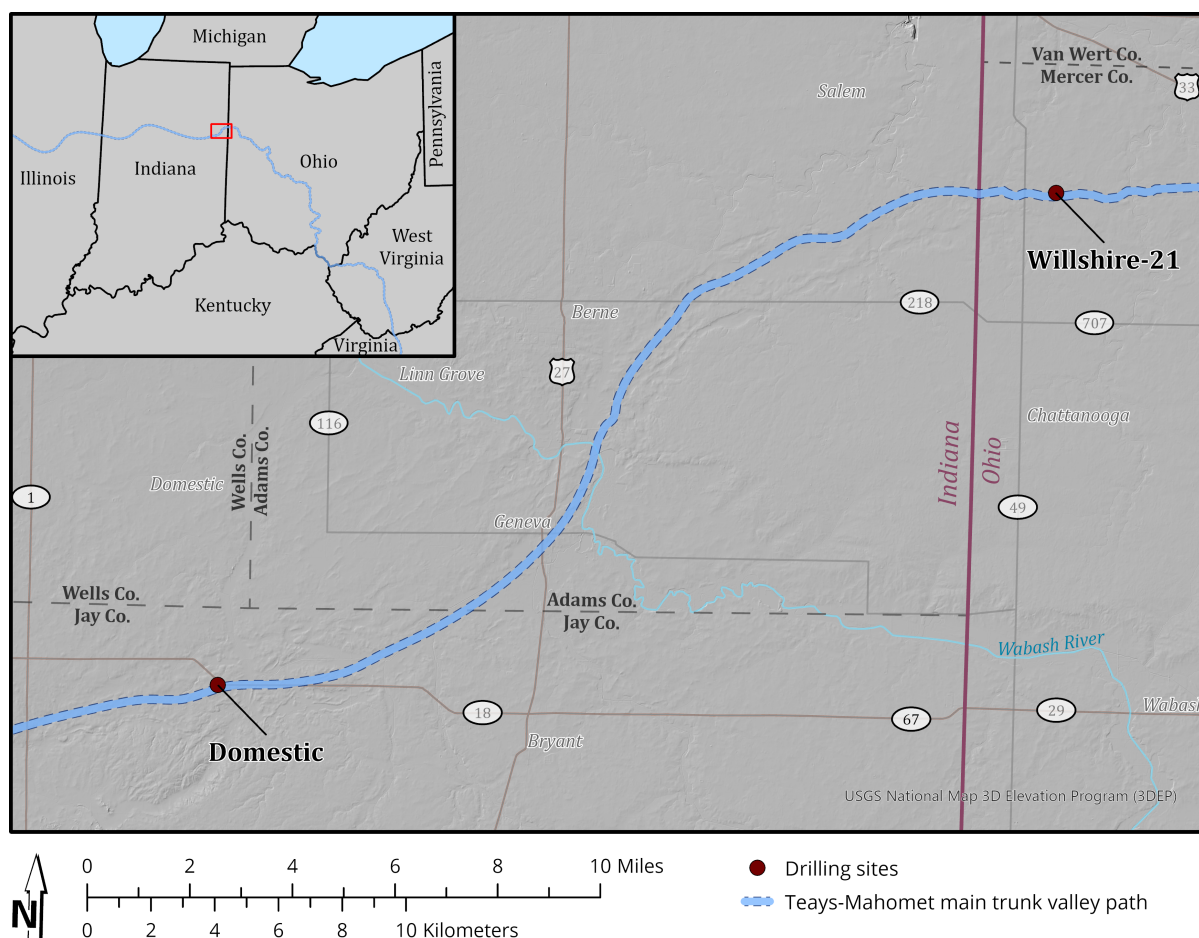


**FIGURE 1.** Map showing the location of the two drilling sites (Willshire-21 and Domestic; dark blue circles) in relation to the main path of the subsurface Teays-Mahomet Valley (thick light-blue line). The inset map (top) indicates the extent of the location map (red) and shows the regional path (blue) of the main Teays-Mahomet Valley.

## METHODS

### Drilling and Core Handling

The field sites in close proximity to the buried Teays Valley system were identified by utilizing passive seismic geophysical results obtained while remapping the bedrock topography at the Ohio and Indiana state border (Nash and others, 2021; Rupp and others, 2021). The cores were drilled by Frontz Drilling from Wooster, Ohio. The continuously drilled, 4-inch-diameter sediment cores were bored using a rotary sonic drill rig. The rotary sonic method was chosen because of its ability to reliably recover a continuous, near-undisturbed sediment core compared to other drilling operations, such as air or mud rotary. The typical rotary sonic drilling process is detailed in figure 2. Extruded 1.5 m (5 ft) core intervals were sheathed into plastic liners and then placed into halved PVC pipes, where they were taped, labeled, and secured for transport. For drilled intervals that were presumed to contain fine-grained sand ideal for Optically Stimulated Luminescence (OSL) dating<sup>3</sup>, 1.5 m (5 ft) core intervals were extruded into black opaque HDPE liners, or were immediately wrapped with black opaque HDPE liners, to prevent exposure to direct light.

<sup>3</sup> OSL samples for these cores were not fully processed during the time of publication.

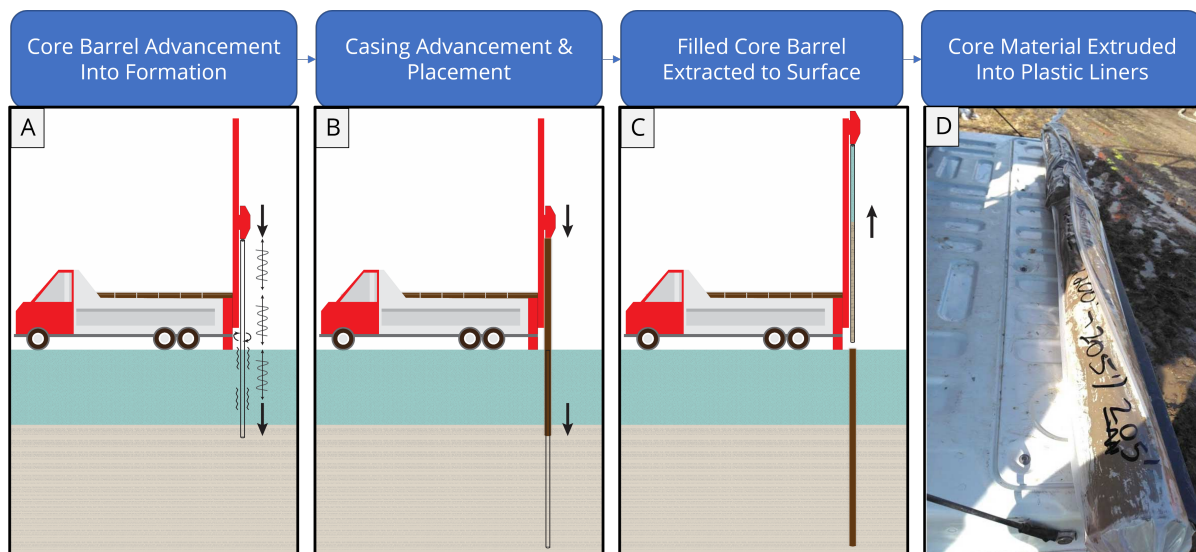


**FIGURE 2. Rotary sonic drilling process. A: The core barrel impacts, rotates, and vibrates at a high frequency to penetrate through the subsurface material. B: A casing is drilled to stabilize the hole. C: The filled core barrel is pulled up to the surface. D: The sonic-cored materials are then extruded directly into plastic liners in approximately 1.5 m (5 ft) intervals.**

Once the hole was completed and stabilized, the drill strings were removed leaving the empty, cased hole. A tripod with a pulley mount was set up above the hole to allow a Mt. Sopris® 2PGA-1000 gamma sonde to descend the hole, which was controlled by a Matrix logging console and mini-winch. The gamma sonde logged continuously down- and then up-hole using methods described in Bleuer (2004). The gamma logs used in this report were obtained from data gathered up-hole at a rate of 1.5 m/minute (5 ft/minute).

After transport to the H. R. Collins Laboratory and Core Repository in Delaware, Ohio, each 1.5 m (5 ft) section of unconsolidated core was cut and split lengthwise by using a combination of cutting wire, hammers, and putty knives to divide the unconsolidated material into two

approximately equal halves. One half was preserved for photography and archiving, and the other half was used for detailed description and subsampling. Archived core halves were placed horizontally onto a core rack stand in groups of sequential 6 m (20 ft) sections (or four drill core runs) for each photo (see [Dataset 1](#) and [2](#)). A set of white studio lights was placed on both sides of the core for appropriate lighting, and windows were covered to block ambient light. The photos were taken using a camera mounted on a tripod positioned directly above the core rack. The remaining non-archived half of the core section was then measured and described by addressing characteristics such as Munsell and general color, lithology, texture, sorting, pebble content, structures, density, contact type, weathering, and secondary features (see [Dataset 3](#) and [4](#)). After writing core descriptions, several samples near the center of the core half were obtained, primarily for PSA and pXRF. Samples were taken at regular intervals, especially in diamicton, to obtain at least one sample for PSA and pXRF for every 1.5 m (5 ft) section. Additional samples were taken before and after lithologic contacts. In sections dominated by very coarse sands and gravels, approximately two large grab samples were taken at different intervals per 1.5 m (5 ft) section in lieu of dedicated PSA or pXRF subsamples. Additional samples were taken for potential future X-Ray Diffraction (XRD) and heavy mineral/geochemistry analyses, possible organics, and other instances of unique intervals. After each archival photo was taken and subsamples were collected, both core halves were prepared for long-term storage by sliding each half-PVC core into clear plastic sleeves and taping each end to create an airtight seal.

### **Portable X-Ray Fluorescence (pXRF)**

Elemental abundances were analyzed via pXRF to determine broad chemical similarities and differences of units within the two Teays cores. Methods of unconsolidated sample preparation and analysis for pXRF vary among authors and detail of study (e.g., Wittkop and others, 2020; Knight and others, 2021), but it is largely agreed that the most reliable data are obtained by first preparing the sample and examining only the dry, homogeneous, fine fraction of the matrix materials to avoid effects from heterogeneous pebble lithologies, variable grain sizes, and moisture effects, as opposed to measuring directly on the unprocessed sample. The Ohio Geological Survey prepared samples for pXRF analysis by first air drying and then oven drying as needed at approximately 45°C (113°F) to remove excess moisture. The samples were then crushed and powdered via mortar and pestle. These powdered subsamples were then sieved to obtain at least 3 grams of the <0.063-mm fraction. The fine-grained samples were poured and compacted into small polyethylene XRF sample cups with 4-micron-thin plastic film covering the bottom for pXRF analysis.

Each sample's elemental composition estimates were obtained in the lab by measuring sample fluorescence after exposure to X-rays. This analysis was performed using the Ohio Geological Survey's pXRF device (Thermo Scientific Niton XL5 XRF Analyzer) attached to a portable test stand. Each sample was analyzed in mining mode for three batches run at 180 seconds. Each sample's elemental percent values were then converted to oxide percent if applicable (i.e., Al, Ca, Fe, K, Mg, P, Si, and Ti). The sample elemental values were then normalized to two measurements of the NIST standard SRM 2709a (Mackey and others, 2010): one standard analysis was performed before and one performed after a set of sample analyses. The SRM 2709a reference standard was chosen for calibration because its reported composition was expected to have the most geochemical similarity to the tested unconsolidated core samples out of the suite of standards available at the time of analysis. Results of the three normalized sample analyses were then averaged to obtain one set of elemental estimates per sample, expressed in mg/kg (ppm). A propagated uncertainty value was then calculated based on the instrument output of two-sigma values for each reading and the calibration standard error (if available). Note that these uncertainty calculations were performed to provide a relative understanding of error, as pXRF data should be considered a semi-quantitative data source in most situations.

### **Particle Size Analysis (PSA)**

Samples for particle size analysis, processed at the Indiana Geological and Water Survey, were first air-dried and then crushed by mortar and pestle. Two methods were used for particle size analysis. Laser diffraction was used for diamicton (till) samples in determination of the matrix grain size and for silty or sandy samples where the maximum grain diameter was <1.4

mm. Clasts >1.4 mm were removed from till samples by sieving prior to analysis. Particle size distribution was determined using laser diffraction on a Malvern® Mastersizer 3000 (see Miller and Schaetzl, 2012). Samples were dispersed with a 5 g/L solution of sodium metaphosphate and subject to 120 seconds of 40 W inline sonication prior to measurement. Samples were run in triplicate using a Hydro EV wet dispersion unit for 40 seconds each with a stirrer speed of 3,000 revolutions per minute. These three runs were averaged for a final result. Mie scattering with a particle refractive index of 1.544, a particle absorption index of 1.0, and a dispersant refractive index of 1.33 (water) was used to determine the final grain size distribution (Wiscombe, 1980). Results from laser diffraction analysis are reported in volume percent. Samples with a maximum grain size of >1.4 mm were sieved at 1 phi ( $\phi$ ) intervals ( $\phi = \log_2 D$ , where D = particle diameter in mm), from -7 to 4 phi (128 mm to 0.063 mm) using a sieve shaker. Results from sieving are reported as mass percent.

## RESULTS

### Core Stratigraphy

Descriptions of the stratigraphy in both cores show that multiple units of Quaternary-aged sediments are present within the buried valley. Simplified stratigraphic columns for each core show the primary lithology with depth and are compared to select physical and chemical results to determine preliminary interpretations (figs. 3 and 4). The Willshire-21 core has a total depth of 160.7 m (335.0 ft) and the bedrock contact was measured at 100.4 m (329.5 ft). The bedrock elevation at the Willshire-21 drill site was calculated to be 147.7 m (484.5 ft) above mean sea level. The Domestic core has a total depth of 121.9 m (400.0 ft), and the bedrock contact was measured at 119.1 m (390.9 ft). The bedrock elevation at the Domestic drill site was calculated to be 146.0 m (478.9 ft) above mean sea level.

### Willshire-21 core stratigraphy

The Willshire-21 core is primarily composed of diamicton, with this material accounting for nearly two-thirds of the total depth of the core (fig. 3). The remaining one-third of the core sediments can be classified either as sand-and-gravel-dominated units interpreted as glaciofluvial packages or as clay-and-silt-dominated units interpreted as glaciolacustrine or lacustrine in origin. Eight major lithologic packages were identified during the description of the Willshire-21 core: four unique diamicton units ( $A_w$ ,  $B_w$ ,  $D_w$ , and  $F_w$ ); two dominantly glaciofluvial units ( $C_w$  and  $G_w$ ); one unit dominated by glaciolacustrine with minor glaciofluvial sand and gravels (Unit  $E_w$ ); and the bottom-most limestone bedrock (Unit  $H_w$ ).

*Unit  $A_w$ .* The first diamicton, Unit  $A_w$ , is found in the upper 23 m (75 ft) of the core and includes the modern soil developed at the ground surface and several thin silt beds within the diamicton. Where unweathered, this diamicton has a variable gray to grayish brown color (10YR 5/2-1 to 10YR 4/2-4/1). The upper diamicton package ( $A_{w1}$ ) is homogenous and massive, containing a silty to silty-clay loam matrix that coarsens slightly with depth, with a moderate to abundant clast content. The lowermost diamicton ( $A_{w2}$ ) within  $A_w$  contains a coarser texture and is structureless.

*Unit  $B_w$ .* Directly below Unit  $A_w$  is an abrupt, thin silt to fine-sand bed that separates the Unit  $A_w$  diamicton and the diamicton in Unit  $B_w$ . This diamicton has a unique very dark grayish-brown to brown color (10YR 3/2; dominantly 10YR 4/2) and is relatively thin (about 5.5 m [18 ft] thick). The diamicton in Unit  $B_w$  is considerably denser than the diamicton in Unit  $A_w$ . Also, Unit  $B_w$  contains a coarser matrix (silt to fine sand) compared to Unit  $A_w$  (clay to silt) with more abundant >2mm clasts. The lower portion of Unit  $B_w$  ends with several interbedded layers of silt and sand.

*Unit  $C_w$ .* The next unit is a coarse, poorly sorted sand-and-gravel package with occasional cobbles. The contact between Unit  $B_w$  and Unit  $C_w$  is abrupt, denoted by the occurrence of a sand-rich zone. Although much of this unit is composed of massive medium- to coarse-grained sands with angular to subangular clasts, it contains several thin beds of well-sorted sand with minor fining upward and coarsening upward sequences. This coarse unit is 18 m (45 ft) thick and ends with gradational contact that grades into diamicton.

*Unit  $D_w$ .* The third diamicton, Unit  $D_w$ , is dark grayish brown (10YR 4/2) with a silty loam textured matrix supporting many angular and subangular pebbles. This unit is the thickest

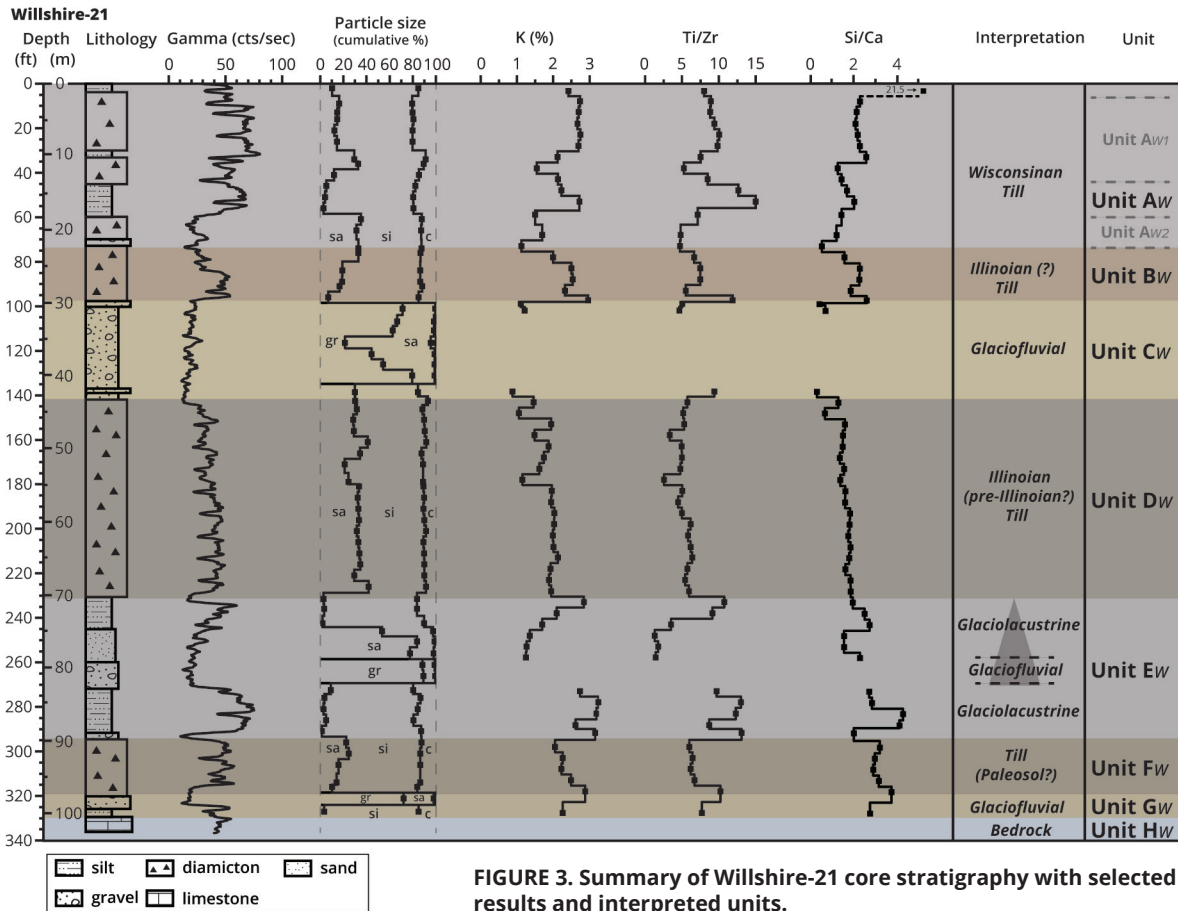


**FIGURE 3.** Summary of Willshire-21 core stratigraphy with selected results and interpreted units.

diamicton unit observed in the core (approximately 27 m [90 ft]) and is homogenous with regards to matrix texture and relative clast abundance. This poorly sorted diamicton contains many similarities with the thinner Unit B<sub>w</sub>, such as having a dark-brown to gray color (10YR 4/2); moderate gravel and cobble content; high density; and silty matrix texture.

*Unit E<sub>w</sub>.* Beneath the diamicton in Unit D<sub>w</sub> is a mix of fine-grained packages and a thinner coarse-grained package, comprising a notable fining upward sequence. The silts and clays within this unit typically have thin laminations and platy structures. Occasional well-sorted fine- to medium-grain sands do not have any observable bedding and have rounded to subangular grains. A very coarse sand-and-gravel-dominated interval (approximately 4 m [12 ft] thick) marks the beginning of the dominantly fining-upward sequence (between 83 m [272 ft] to 70 m [231 ft]). Below this sand and gravel is an abrupt contact with a clay-and-silt interval similar to the upper portion of this unit, with occasional distorted laminae and thin fine-sand intervals.

*Unit F<sub>w</sub>.* The final, lowermost diamicton exhibits a dark reddish-gray color (5YR 4/2) which grades into a brown color (7.5YR 4/2) after 3 m (10 ft) in depth. The contact is abrupt between Units E<sub>w</sub> and F<sub>w</sub>. The variably fine-to-coarse matrix is calcareous and has a blocky, massive matrix with many indications of redox and weathered clasts. The fresh material also gave off an organic gaseous odor.

*Unit G<sub>w</sub>.* Underneath Unit F<sub>w</sub> is a thin, poorly sorted muddy sand-and-gravel package with a mix of rounded to angular gravels and cobbles. A thin, gravel-rich, very poorly sorted, sandy diamicton-like material transitions into mixed clays and fine sands that composes the end of the unit.

*Unit H<sub>w</sub>.* The bottommost unit contains a mostly weathered and pulverized white to blueish-gray limestone. The contact between Unit G<sub>w</sub> and Unit H<sub>w</sub> is abrupt, representing the unconformity between the underlying Paleozoic bedrock (likely Ordovician Whitewater Formation, Unit H<sub>w</sub>) and the overlying Quaternary-aged unconsolidated sediments (Units A<sub>w</sub>–G<sub>w</sub>).

**Domestic core stratigraphy**

The Domestic core is composed primarily of several coarse sand-and-gravel packages and finer sands to silt-and-clay packages, interpreted as transitions between glaciofluvial outwash and glaciolacustrine depositional environments, respectively (fig. 4). Diamicton accounts for only the upper quarter of the entire core. Six major lithologic packages were identified during the description of the Domestic core: two unique diamicton units ( $A_D$  and  $B_D$ ); one dominantly glaciolacustrine unit with potentially underlying deltaic deposits ( $C_D$ ); one unit dominated by glaciofluvial sands and gravels ( $D_D$ ); a mixture between primarily glaciofluvial and glaciolacustrine cycles ( $E_D$ ); and the bottommost limestone bedrock unit ( $F_D$ ).

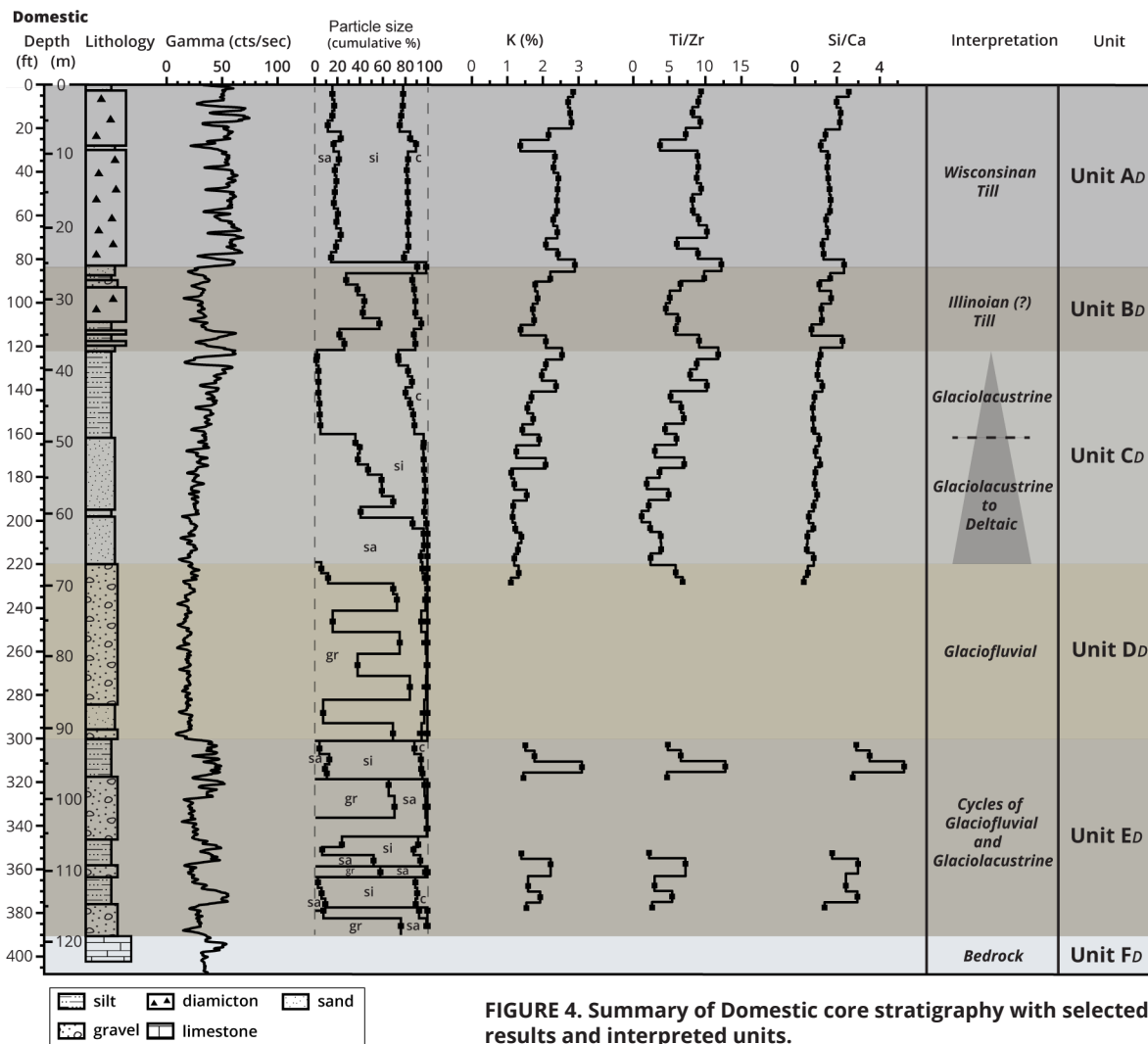


**FIGURE 4. Summary of Domestic core stratigraphy with selected results and interpreted units.**

*Unit  $A_D$ .* Unit  $A_D$  contains the first diamicton and is found in the upper 26 m (85 ft) of the core; it includes modern soil developed at the ground surface. The upper 6 m (21 ft) of the diamicton contains indications of oxidation and weathering. Below this partially weathered upper portion, the matrix has a dark gray to grayish brown color (10YR 3/1 to 10YR 4/2) and is calcareous. Overall, this diamicton unit has a homogenous silty to silty-clay loam matrix with moderate to abundant clast content with occasional thin beds of silt and fine sand.

*Unit  $B_D$ .* Directly below Unit  $A_D$  is Unit  $B_D$ , comprising the second and last major diamicton encountered in the core. The contact between Unit  $A_D$  and Unit  $B_D$  is abrupt, denoted by several feet of tan, fine-to-medium-grained sands and silts. The diamicton in Unit  $B_D$  is thinner (approximately 4 m [12 ft]) and notably denser than the overlying diamicton (Unit  $A_D$ ) and is a very dark-gray color (10YR 3/1 to 10YR 4/1). Unit  $B_D$  also contains a massive, coarser matrix

(silt to fine sand) with more abundant >2mm clasts compared to the overlying Unit A<sub>D</sub>. The lower portion of Unit B<sub>D</sub> ends with several interbedded layers of silt and sand.

*Unit C<sub>D</sub>.* The coarser sands at the bottommost section of Unit B<sub>D</sub> quickly transition into Unit C<sub>D</sub>, a dominantly fine-grained, fining upward sequence dominated by thick clay and silt and fine sands. The upper 12 m (40 ft) of Unit C<sub>D</sub> contains homogenous, massive, and calcareous clays and silts (10YR 4/2 to 10YR 4/1). This finer package gradually grades into a coarser silt to fine- to medium-grained sand with depth (about 18 m [58 ft] thick). The sands are massive and very well sorted, occasionally containing thin laminated silty clay layers that alternate colors between laminae (10YR 4/1 and 10YR 3/1). Also within this lower subunit are small packages of coarser sands and trace gravels.

*Unit D<sub>D</sub>.* Unit C<sub>D</sub> unevenly grades into Unit D<sub>D</sub>, which is approximately 24 m (80 ft) of coarse sand and gravels. This coarse unit is massive with no observable bedding or stratification. Sand-dominated intervals are well sorted and calcareous. Rounded and subrounded pebbles are found all throughout the unit and are dominantly carbonate, shale, or Canadian Shield (igneous/metamorphic) lithologies.

*Unit E<sub>D</sub>.* Unit E<sub>D</sub> contains characteristics similar to Unit C<sub>D</sub> and Unit D<sub>D</sub> but contains a mixture of thinner packages of dominantly fine and dominantly coarse cycles: three silt-clay intervals and three sand-gravel intervals. The contact between E<sub>D</sub> and the overlying Unit D<sub>D</sub> is considered abrupt (between two core runs). The silt-and-clay intervals are each massive, calcareous, and have a similar dark gray-brown (10YR 4/2) color as Unit C<sub>D</sub>. The sand-and-gravel intervals are each moderately sorted, lack bedding, with well-rounded pebbles that are carbonate and Canadian Shield lithologies. However, between 105 m (346 ft) and 106 m (349 ft) there is evidence of a clast-dominated diamicton with a silty matrix. This diamicton separates a coarse and fine sequence, with gradual upper contact (with sand and gravel) and a sharp lower contact (with clay and silt).

*Unit F<sub>D</sub>.* The lowermost unit contains the bedrock contact at a depth of approximately 119 m (391 ft). The contact between the consolidated bedrock and the overlying unconsolidated sand and gravel (Unit E<sub>D</sub>) is fairly abrupt, with mostly well-rounded carbonate pebbles and muddy diamicton-like masses found at the base of the unconsolidated. The weathered carbonate bedrock is mostly a white to gray pulverized Upper Ordovician-aged limestone.

## pXRF Results

The calculated estimate of the abundance of the 45 elements was obtained for 112 total sampled intervals (n = 57 for Willshire-21; n = 55 for Domestic; Appendix 1). For the 45 elements analyzed, 21 elements were consistently below the level of detection for both cores (<LOD; Ag, Au, Bi, Cd, Cl, Co, Hf, Hg, Mo, Nb, Pd, Pr, Re, S, Sb, Se, Sn, Ta, U, W, and Y), and six elements had relatively high percent uncertainty (>30%; Ba, Cr, Mn, Ni, P, and V). Of the remaining 18 elements, three elements typically exhibited highly variable readings among the triplicate analysis for the sample (i.e., the percent difference between readings of the same sample tended to be much greater than the percent uncertainty; Mg, Nd, and Zn). We chose 16 elements to plot and compare for further analysis (fig. 5; Appendix; Al, As, Ca, Cu, Ce, Fe, K, La, Mg, Pb, Si, Sr, Rb, Th, Ti, and Zr).

The 16 selected elements can be categorized into several major groups based on elemental abundance. Elements Si and Ca displayed the highest range of abundances overall, generally ranging from >10,000 to >100,000 ppm. Elements with intermediate values (<100,000 ppm) include Al, K, Fe, and Mg. Excluding Ti, which ranged from approximately 500 to 3,000 ppm, the remaining minor elements (Cu, Sr, Zr, As, Ce, La, Pb, Rb, Th) were typically <500 ppm; As, Ce, La, Pb, Rb, and Th were consistently <160 ppm. Both cores displayed similar magnitudes of these elemental abundances but were variable overall.

Although the accuracy of the elemental values obtained from pXRF analysis varies by element and concentration level, the relative change from one sample to the next indicates important trends with depth that can be used in interpretation. While variable in abundance, many elements exhibited similar or conflicting trends with depth, likely based on mineralogy. Broadly, especially in the case of Si and Ca, these associations may be related to dominance in siliclastic or calcium carbonate source materials with variable contribution to igneous and metamorphic lithologies from eroded and weathered glacial erratics. Many elements mirrored

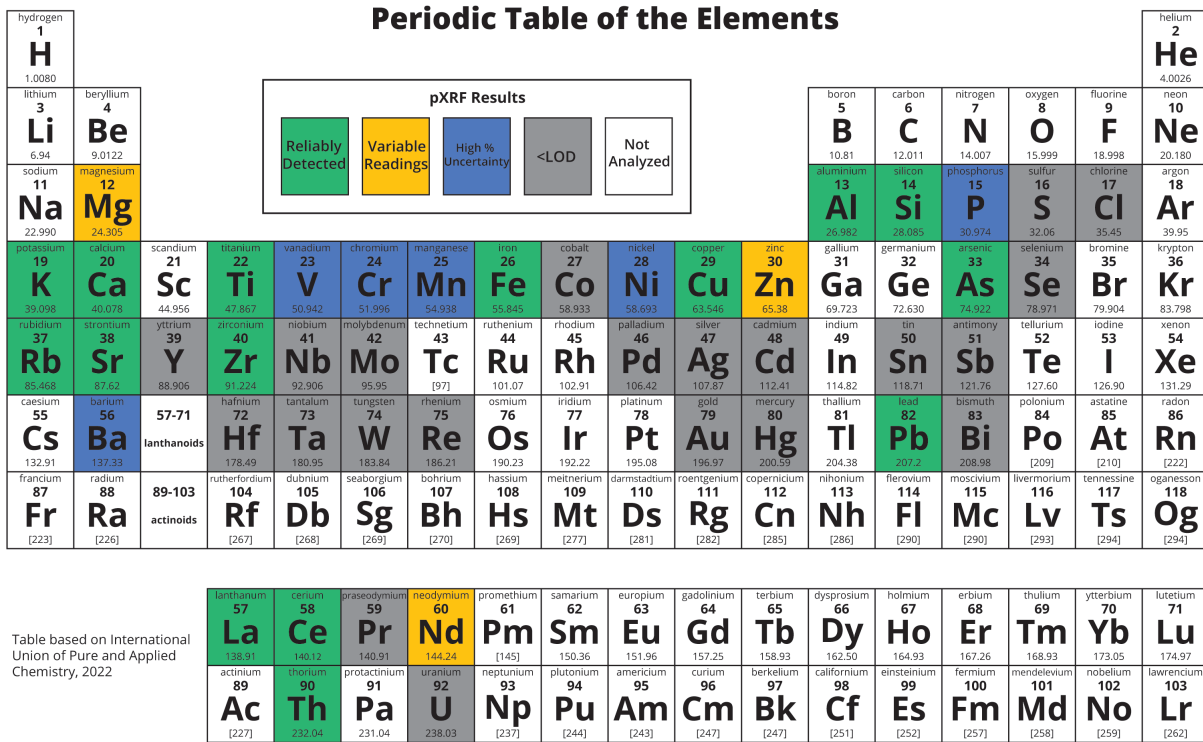
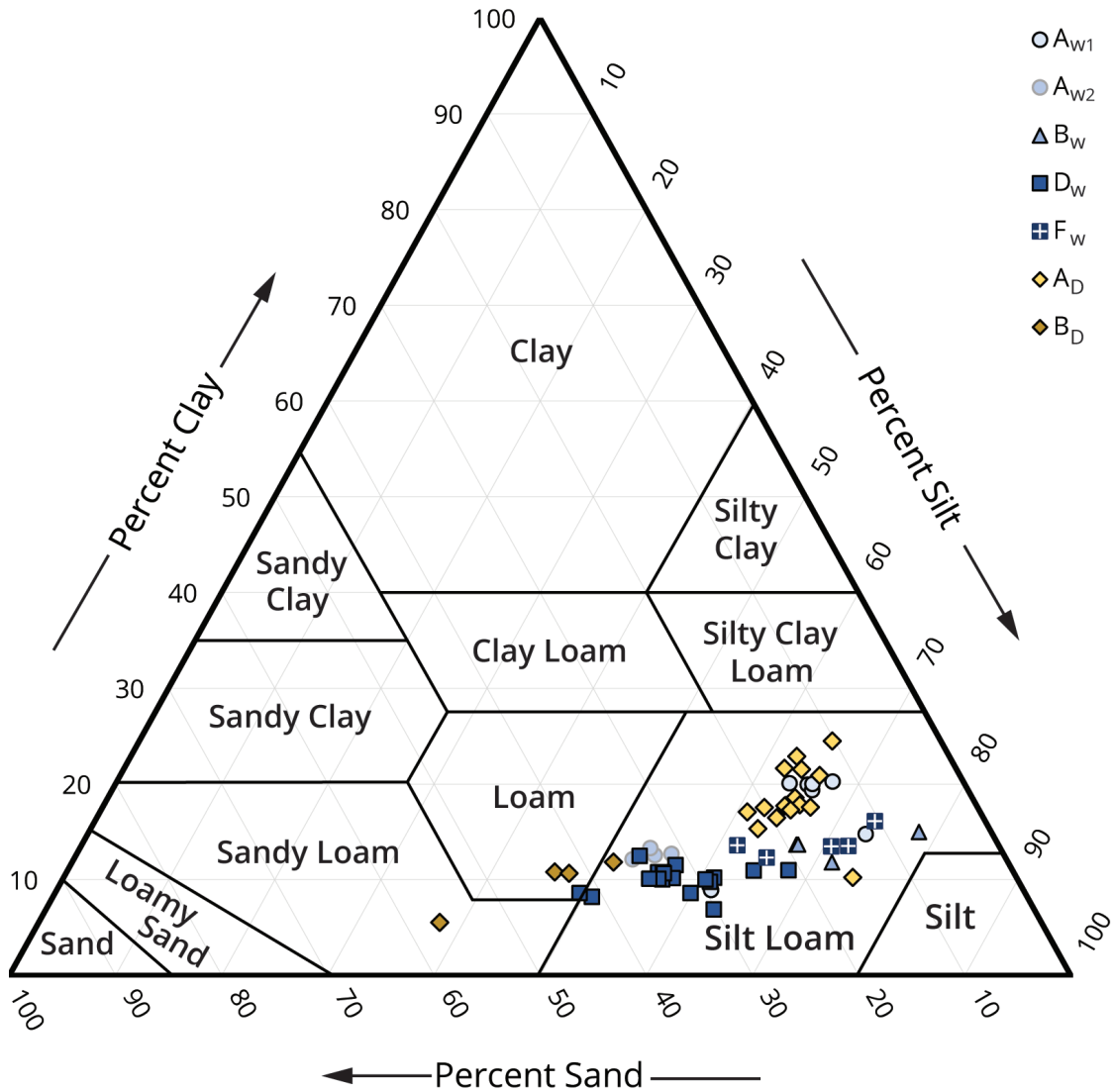


**FIGURE 5. Elements visually categorized on a periodic table based on pXRF results. Elements in green were reliably detected and plotted for further analysis. Dark yellow elements had relatively variable readings and were not included for further analysis. Blue elements had high percentages of uncertainty and were not included for further analysis. Gray elements were consistently below the level of detection and were not included for further analysis.**

the trends of either Si or Ca. The ratios between some elements may indicate similarities or differences between source materials and may also indicate textural differences. For example, the most homogeneous unit for many elements is Unit  $D_w$  in Willshire-21. Unit  $D_w$  is the thickest and most uniform till unit with minor variations for most elements, notably Ti/Zr and Si/Ca, implying a consistent parent material homogeneity. The percentage of elements, such as K, compared to the total analysis also follow similar relationships with depth.

**PSA Results**

A total of 136 particle size analyses were performed (Willshire-21 n = 66; Domestic n = 70). These data were plotted as cumulative percent and were categorized by percent gravel, sand, silt, and clay, if applicable. These relative trends aided in unit identification and interpretation. Obvious increases in sand and gravel corresponded to instances of outwash or glaciofluvial packages, whereas silt-and-clay-dominated samples were mainly from a more glaciolacustrine setting. Grain-size distributions are largely supported by gamma-ray log data, but trends with depth and averages within units provide quantifiable textural information within the sand-silt-clay matrix fraction, especially with diamicton units, that refine and support observations (fig. 6). Diamicton in both cores are mostly determined to be of a silt loam texture, with slight decrease in clay content with depth. Two diamicton intervals in Unit  $A_w$  ( $A_{w1}$  and  $A_{w2}$ ) were separated by a notable silt package and were plotted separately to show differences in texture. At a glance, the youngest, uppermost diamicton units ( $A_{w1}$  in Willshire-21 and  $A_D$  in Domestic) in both cores are texturally similar; but others, such as the sandier unit  $B_D$  (in Domestic), appear to be unique. Additional grain size analysis data are found in Appendix 2.



Core	Unit	Top Depth (ft)	Bottom Depth (ft)	Average % Sand	Average % Silt	Average % Clay
Willshire-21	A <sub>w1</sub>	8.94	40.98	18.31	64.82	16.71
Willshire-21	A <sub>w2</sub>	60.82	75.98	33.08	54.22	12.70
Willshire-21	B <sub>w</sub>	83.94	95.98	15.32	71.13	13.55
Willshire-21	D <sub>w</sub>	142.54	225.98	32.03	57.90	10.07
Willshire-21	F <sub>w</sub>	295.98	315.98	17.49	68.69	13.82
Domestic	A <sub>D</sub>	3.94	78.94	16.86	64.57	18.41
Domestic	B <sub>D</sub>	93.61	109.27	44.72	45.53	9.74

FIGURE 6. USDA (United States Department of Agriculture) texture ternary diagram plot of selected PSA samples of major diamicton units (top) and average grain size data for major diamicton units within both cores (bottom). See figures 3 and 4 for stratigraphy and particle information.

## DISCUSSION

The addition of the Domestic and Willshire-21 cores helps to expand the established regional stratigraphic framework of the Lafayette and Teays systems. Sediments preserved within the valley span multiple glacial episodes and therefore represent a more complete account of regional glacial history, relative to nearby upland areas. A comparison of the core stratigraphy with relation to previously published models of the bedrock surface further depict the differences in valley fill and morphology (figs. 7 and fig. 8). This complex glacial history is evidenced by the remarkably differing unconsolidated sediment packages between the two cores. Willshire-21 contains dominantly diamicton units with relatively thin lacustrine and outwash units, whereas Domestic contained less diamicton overall but is dominated by several thicker sequences of glaciolacustrine and outwash. These findings confirm that the buried bedrock system is filled with inconsistent unconsolidated deposits that vary even within a span less than 32 kilometers (20 miles). Within the study area, the eastern portion of the valley (Willshire-21) contains strong evidence of glaciogenic materials directly deposited by ice (i.e., tills), whereas the western portion of the valley (Domestic) contains more evidence of materials deposited by water (i.e., glaciofluvial sands and gravels and silts and clays related to suspension settling). This evidence refines the subglacial-proglacial transition interpretation from Bleuer (1991), which suggests lake ice-damming at bends in the valley near the Ohio-Indiana state border (i.e., the Marion Valley section). Continued drilling with additional physical, chemical, and age data within the buried Teays system is needed to fully detail correlations between cores and regional glacial frameworks.

## CONCLUSIONS AND FUTURE WORK

The data presented in this report provide additional evidence for the variable nature of the buried Teays-Mohamet Valley fill and can be used to support detailed Teays stratigraphy and regional Quaternary studies in the future. Future works can correlate the upper till units and some of the glaciolacustrine and glaciofluvial events into a regional framework. Much of the Teays Valley fill is unique between these two borings, and the unit sequences also differ from previous core stratigraphy works within the Teays. These findings warrant a more detailed analysis of not only the material recovered from this project, but the need for additional deep borings within the Teays.

Future studies could more rigorously test physical and chemical properties of the Willshire-21 and Domestic cores to support regional Quaternary stratigraphic frameworks and an in-depth understanding of the Teays Valley history. Continued work on elemental data can identify trends with other core characteristics by running more samples with other analysis techniques, such as conventional X-Ray Fluorescence (XRF), Inductively Coupled Plasma Mass Spectrometry (ICP-MS), or X-Ray Diffraction (XRD) data. The pXRF data provided in this report may help guide desired target zones for such analyses. Multiple XRD samples were obtained during this project but were in-progress during the time of publication (data forthcoming). Geochemical data combined with particle size data can aid in the classification of till units and glacial events. Such glacial events can be interpreted with age constraints through additional age-dates from OSL dating, radiocarbon dating, and other techniques. Several OSL samples were obtained during this project but are preliminary and in-progress during the time of publication (data forthcoming). The data presented in this report are intended to provide a reference and guide for future work to understanding the Teays Valley development and regional glacial history.

## ACKNOWLEDGEMENTS

The authors thank the Great Lakes Mapping Coalition (Cooperative Agreement Number G20AC00302) for the funds and opportunity to work on the project. The completion of this report was possible with support from the Ohio and Indiana State Geologists. We also thank staff who assisted with the project during drilling, core handling, and sample prep and analysis, including but not limited to: Jeffery Deisher (ODNR), Brittany Parrick (ODNR), Samuel Hulett (ODNR), and Thomas Valachovics (ODNR). Special thanks go to the landowners who allowed drilling on their properties and to the drill crew at Fronz Drilling who efficiently drilled for many days and accommodated us in the field.

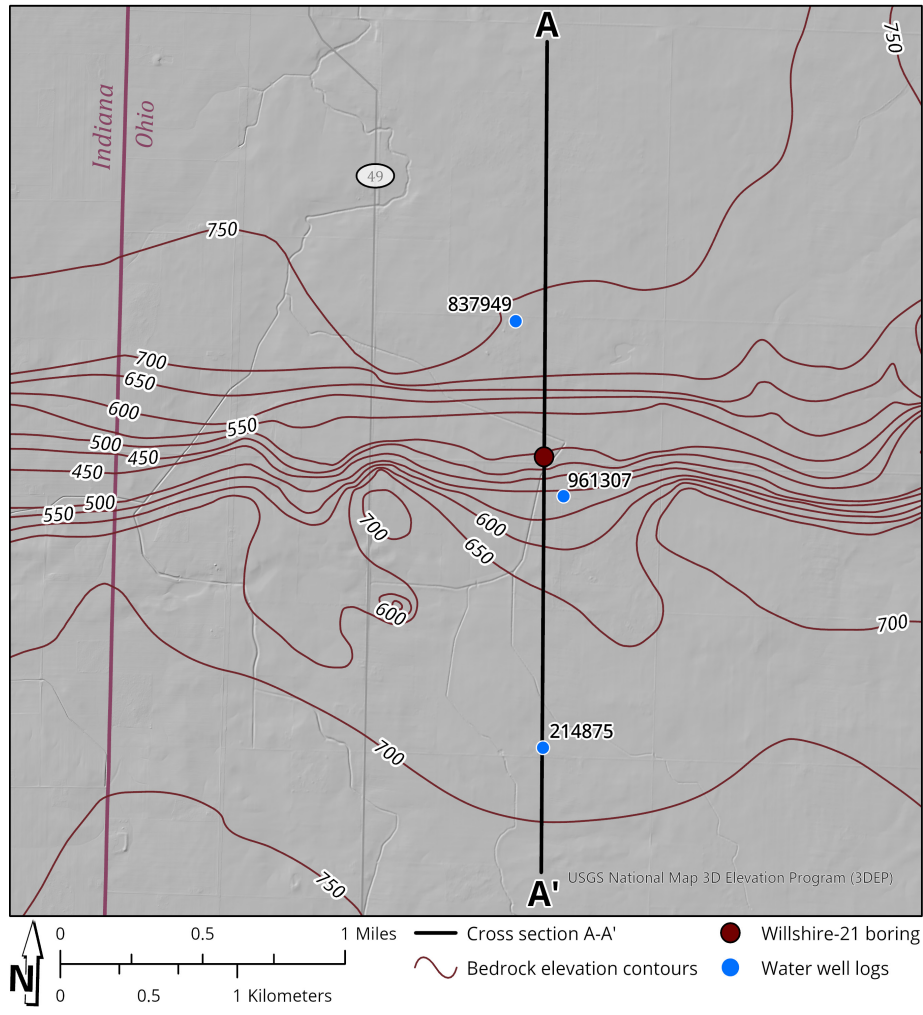
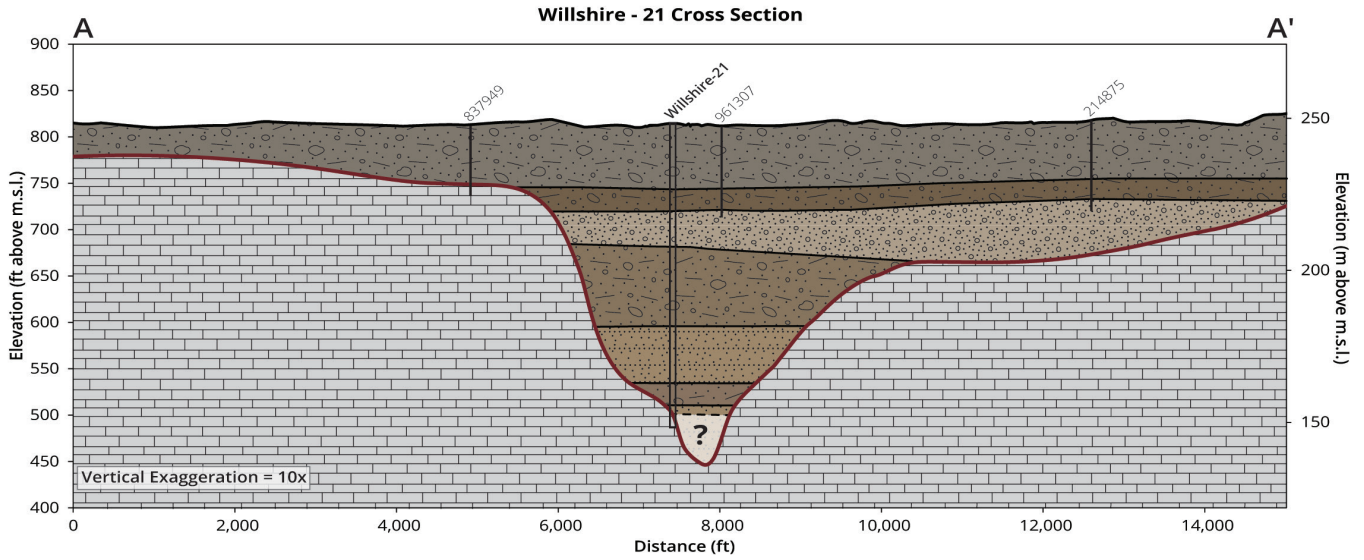


**FIGURE 7. Cross section of Willshire-21 based on major stratigraphic units (top) and reference map (bottom). Bedrock surface contact modeled from previous mapping efforts (Rupp and others, 2021; Nash and others, 2021). The bottommost section of the buried Teays valley (thalweg) was not drilled through and is lacking lithologic information ("?") but is inferred to be composed of sand-and-gravel similar to Unit Gw. Reliable water wells within approximately 305 m (1,000 ft) perpendicular to the cross-section line are labeled by record number (ODNR, 2022).**

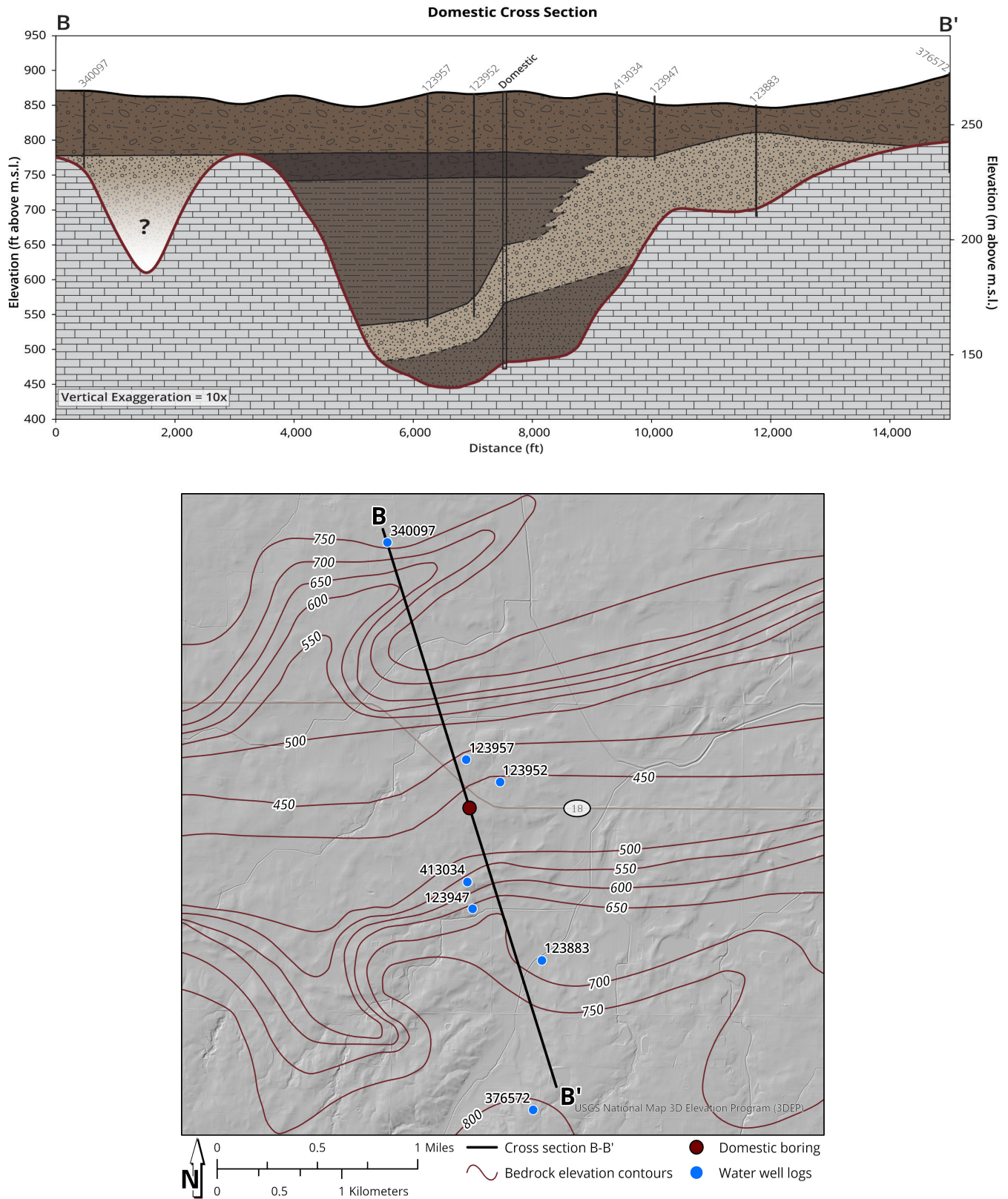


**FIGURE 8.** Cross section of Domestic based on major stratigraphic units (top) and reference map (bottom). Bedrock surface contact modeled from previous mapping efforts (edited from Rupp and others, 2021). The modelled buried valley to the northwest of the Domestic boring is lacking lithologic information (“?”) but may be filled with sand-and-gravel based on the nearby well log (ID 340097). Reliable water wells within approximately 305 m (1,000 ft) perpendicular to the cross-section line are labeled by record number (IDNR, 2019).

## REFERENCES

- Bleuer, N.K., 1991, The Lafayette Bedrock Valley System of Indiana; concept, form, and fill stratigraphy, *in* Melhorn, W.N., and Kempton, J.P., eds., *Geology and hydrogeology of the Teays-Mahomet Bedrock Valley System: Geological Society of America Special Paper 258*, Boulder, Colorado, p. 51–77.
- Bleuer, N.K., 2004, Slow-logging subtle sequences—the gamma-ray log character of glaciogenic and other unconsolidated sedimentary systems: *Indiana Geological Survey Special Report 65*, 39 p.
- Bonnett, R.B., Noltimier, H.C., and Sanderson, D.D., 1991, A paleomagnetic study of the early Pleistocene Minford Silt Member, Teays Formation, West Virginia, *in* Melhorn, W.N., and Kempton, J.P., eds., *Geology and hydrogeology of the Teays-Mahomet Bedrock Valley System: Boulder, Colorado, Geological Society of America Special Paper 258*, p. 9–18.
- Bownocker, J.A., 1899, A deep pre-glacial channel in western Ohio and Eastern Indiana: *The American Geologist* vol. 23, p. 178–182.
- Buylaert, J.P., Jain, M., Murray, A.S., Thomsen, K.J., Thiel, C., and Sohbaty, R., 2012, A robust feldspar luminescence dating method for Middle and Late Pleistocene sediments: *Boreas*, v. 41, no. 3, p. 435–451.
- Durcan, J.A., King, G.E., Duller, G.A.T., 2015, DRAC—Dose rate and age calculator for trapped charge dating: *Quaternary Geochronology*, v. 28, p. 54–61. doi:10.1016/j.quageo.2015.03.012.
- Erjavec, J.L., 2018, A new map of Pleistocene proglacial Lake Tight based on GIS modeling and analysis: *Ohio Journal of Science* v. 118, no. 2, p. 57–65. <http://dx.doi.org/10.18061/ojs.v118i2.6548>
- Galbraith, R.F., Roberts, R.G., Laslett, G.M., Yoshida, H., and Olley, J.M., 1999, Optical dating of single and multiple grains of quartz from Jinmium rock shelter, northern Australia—Part I, experimental design and statistical models: *Archaeometry*, v. 41, no. 2, p. 339–364.
- Goldthwait, R.P., 1991, The Teays valley problem: a historical perspective, *in* Melhorn, W.N. and Kempton, J.P., eds., *Geology and hydrogeology of the Teays-Mahomet Bedrock Valley System: Geological Society of America Special Paper 258*, Boulder, Colorado, p. 3–8.
- Gray, H.H., 1982, Map of Indiana showing topography of the bedrock surface: *Indiana Geological Survey, Miscellaneous Map 35*, scale 1:500,000.
- Horberg, L., 1945, A major buried valley in East-Central Illinois and its regional relationships: *The Journal of Geology* v. 53, no. 5, p. 349–361.
- Hoyer, M.C., 1976, Quaternary valley fill of the abandoned Teays drainage system in southern Ohio: Columbus, The Ohio State University, Ph.D dissertation, 163 p.
- Indiana Department of Natural Resources, Division of Water, Resource Assessment Section (IDNR), 2019, WATERWELLS\_IDNR\_IN.SHP: Water well locations in Indiana: 1:24,000, point shapefile.
- Knight, R.D., Kjarsgaard, B.A., and Hazen R.A.J., 2021, An analytical protocol for determining the elemental chemistry of Quaternary sediments using a portable X-ray fluorescence spectrometer: *Applied Geochemistry*, v. 131, 15 p.
- Jacobs, P.M., Mason, J.A., and Hanson, P.R., 2011, Mississippi Valley regional source of loess on the southern Green Bay Lobe land surface, Wisconsin: *Quaternary Research*, v. 75, p. 574–583.
- Jacobson, R.B., Elston, D.P., and Heaton, J.W., 1988, Stratigraphy and magnetic polarity of the high terrace remnants in the Upper Ohio and Monongahela Rivers in West Virginia, Pennsylvania, and Ohio: *Quaternary Research*, v. 29, p. 216–232.
- Mackey, E.A., Christopher, S.J., Lindstrom, R.M., Long, S.E., Marlow, A.F., Murphy, K.E., Paul, R.L., Popelka-Filcoff, R.S., Rabb, S.A., Sieber, J.R., Spatz, R.O., Tomlin, B.E., Wood, L.J., Yen, J.H., Yu, L.L., R. Zeisler, Wilson, S.A., Adams, M.G., Brown, Z.A., Lamothe, P.L., Taggart, J.E., Jones, C., and Nebelsick, J., 2010, Certification of three NIST renewal soil standard reference materials for element content—SRM 2709a San Joaquin Soil, SRM 2710a Montana Soil I, and SRM 2711a Montana Soil II: *National Institute of Standards and Technology, Gaithersburg, Maryland, NIST Special Publication 260-172*.
- Miller, B.A., and Schaetzl, R.J., 2012, Precision of soil particle size analysis using laser diffractometry: *Soil Science Society of America Journal*, v. 76, p. 1719–1727.

- Moore, D.M., and Reynolds, Jr., R.C., 1989, X-ray diffraction and the identification and analysis of clay minerals: Oxford University Press, 322 p.
- Nash, T.A., Norris, T.A., Rupp, R.F., Tripp, D.C., Antinao, J.L., and Loope, H.M., 2021, Bedrock topography of the Willshire 7.5-minute quadrangle, Ohio-Indiana: Columbus, Ohio Department of Natural Resources, Division of Geological Survey Digital Map Series SG-4B, scale 1:24,000.
- Norris, S.E., and Spicer, H.C., 1958, Geological and geophysical study of the preglacial Teays Valley in west-central Ohio, *in* Contributions to the Hydrology of the United States 1956–1959: Washington, U.S. Geological Survey, Water-Supply Paper 1460, 435 p.
- Ohio Department of Natural Resources Division of Geological Survey, 2022, Water Wells Database, last accessed June 30, 2022 at <<https://waterwells.ohiodnr.gov>>.
- Prescott, J.R. and Hutton, J.T., 1994, Cosmic ray contributions to dose rates for luminescence and ESR dating—large depths and long-term time variations: *Radiation Measurements*, v. 23, p. 497–500.
- Rupp, R.F., Tripp, D.C., Antinao, J.L., Loope, H.M., Johnson, M.R., Nash, T.A., and Norris, T.A., 2021, Bedrock elevation of the Berne, Domestic, Geneva, and Willshire 7.5-minute quadrangles, Indiana-Ohio: Indiana Geological and Water Survey, *Indiana Journal of Earth Sciences*, v. 3, scale 1:48,000. doi: 10.14434/ijes.v3i1.31742.
- Stout, Wilber, Ver Steeg, Karl, and Lamb, G.F., 1943, *Geology of water in Ohio*: Columbus, Ohio Department of Natural Resources, Division of Geological Survey Bulletin 44, 694 p.
- Teller, J.T., and Goldthwait, R.P., 1991, The Old Kentucky River; A major tributary to the Teays River, *in* Melhorn, W.N., and Kempton, J.P., eds., *Geology and hydrogeology of the Teays-Mahomet Bedrock Valley System*: Geological Society of America Special Paper 258, Boulder, Colorado, p. 29–41.
- Tight, W.G., 1903, Drainage modifications in southeastern Ohio and adjacent parts of West Virginia and Kentucky: U.S. Geological Survey Professional Paper 13, 111 p.
- Udden, J.A., 1914, Mechanical composition of clastic sediments: *Geological Society of America Bulletin* v. 25, no. 1, p. 655–744.
- Wayne, W.J., 1956, Thickness of drift and bedrock topography of Indiana north of the Wisconsin glacial boundary: *Indiana Geological Survey Progress Report* 7, 70 p.
- Wentworth, C.K., 1922, A scale of grade and class terms for clastic sediments: *The Journal of Geology*, v. 30, no. 5, p. 377–392.
- Wiscombe, W.J., 1980, Improved Mie scattering algorithms: *Applied Optics*, v. 19, p. 1505–1509.
- Wittkop, C., Bartley, J.K., Krueger, R., Bouvier, A., Georg, R.B., Knaeble, A.R., St. Clair, K., Piper, C., Breckenridge, A., 2020, Influence of provenance and transport process on the geochemistry and radiogenic (Hf, Nd, Sr) isotopic composition of Pleistocene glacial sediments, Minnesota, USA: *Chemical Geology*, v. 532, 17 p.
- Wolfe, J.N., 1942, Species isolation and a proglacial lake in southern Ohio: *Ohio Journal of Science*, v. 42, p. 2–12.

Calculated elemental values are provided in terms of parts-per-million (ppm)

Elements Ag, Au, Bi, Cd, Cl, Co, Hf, Hg, Mo, Nb, Pd, Pr, Re, S, Sb, Se, Sn, Ta, U, W, and Y were consistently below the level of detection (<LOD) for both cores

Table A1-1. Willshire-21 pXRF table showing calculated average elemental values and associated uncertainties with depth.

Table with columns for Core, Depth (m), Depth (ft), and various elements (Al, As, Ba, Ca, Ce, Cr, Cu, Fe, K, La, Mg, Mn, Ni, P, Pb, Rb, Si, Sr, Th, Ti, Zn, Zr) with their respective values and uncertainties.

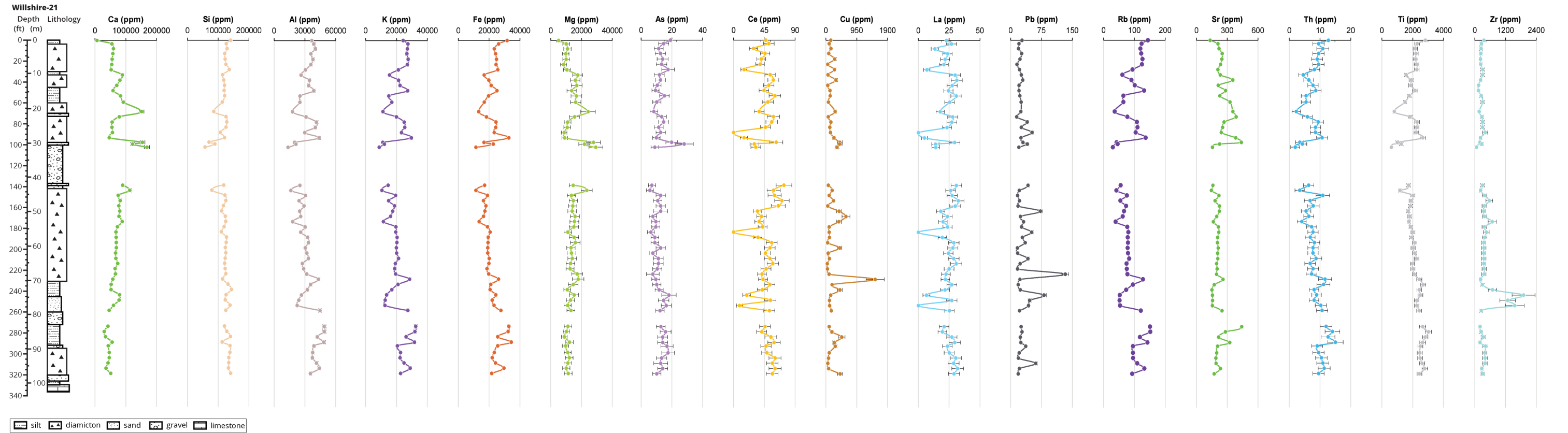


Figure A1-1. Willshire-21 pXRF plot of selected elements.

Calculated elemental values are provided in terms of parts-per-million (ppm)

Elements Ag, Au, Bi, Cd, Cl, Co, Hf, Hg, Mo, Nb, Pd, Pr, Re, S, Sb, Se, Sn, Ta, U, W, and Y were consistently below the level of detection (<LOD) for both cores

Table A1-2. Domestic pXRF table showing calculated average elemental values and associated uncertainties with depth.

Core	Depth (m)	Depth (ft)	Al	Al +/-	As	As +/-	Ba	Ba +/-	Ca	Ca +/-	Ce	Ce +/-	Cr	Cr +/-	Cu	Cu +/-	Fe	Fe +/-	K	K +/-	La	La +/-	Mg	Mg +/-	Mn	Mn +/-	Nd	Nd +/-	Ni	Ni +/-	P	P +/-	Pb	Pb +/-	Rb	Rb +/-	Si	Si +/-	Sr	Sr +/-	Th	Th +/-	Ti	Ti +/-	V	V +/-	Zn	Zn +/-	Zr	Zr +/-
Domestic	1.00	3.28	40543.19	1434.20	13.42	2.87	442.39	316.13	51309.59	2462.79	25.42	5.51	65.77	42.73	64.32	12.13	25223.07	549.49	28495.72	862.49	12.70	2.84	7324.20	1624.75	436.39	457.92	10.24	1.65	38.99	9.03	155.54	72.11	17.09	1.57	131.27	4.77	130609.40	1880.43	155.85	4.15	9.29	1.60	2173.31	149.42	127.09	59.70	96.83	6.07	230.72	54.49
Domestic	2.42	7.95	37934.87	1378.64	10.50	2.50	512.93	366.79	62890.57	3017.01	41.13	7.15	63.98	41.74	147.53	25.81	23876.70	522.17	27139.84	822.38	19.88	3.57	9395.66	1993.72	<LOD	<LOD	15.47	2.04	32.78	9.07	149.21	65.00	48.77	3.99	123.20	4.54	124036.25	1799.12	199.65	5.24	8.48	1.54	1994.25	139.25	124.46	59.31	100.36	6.83	221.42	52.30
Domestic	3.95	12.95	38015.00	1352.57	10.50	2.49	509.62	364.02	56528.12	2713.03	43.41	8.10	79.11	46.26	47.86	10.38	23655.05	516.73	27708.03	839.46	22.35	4.05	9416.60	2087.22	<LOD	<LOD	16.92	2.21	33.62	9.33	154.01	64.65	20.81	1.75	125.73	4.62	121975.99	1761.13	265.04	6.88	8.98	1.67	2033.87	140.25	129.39	59.22	85.36	5.54	248.46	58.68
Domestic	5.27	17.30	39941.40	1418.24	10.18	2.68	510.93	365.04	58087.29	2787.09	47.06	7.84	76.68	44.88	125.91	23.01	23345.61	508.82	28099.56	850.48	21.64	3.70	11605.26	2566.66	<LOD	<LOD	16.38	2.01	36.15	9.61	155.96	66.55	24.79	1.84	126.13	4.63	123318.41	1780.12	208.06	5.45	8.63	1.75	2021.72	139.93	118.34	54.11	92.33	5.90	217.07	51.28
Domestic	7.00	22.95	32819.35	1246.08	10.39	2.60	470.24	336.39	81698.09	3915.75	44.59	7.56	52.80	40.10	40.96	9.77	19872.30	436.54	21614.42	658.07	24.52	4.34	13793.05	2767.03	<LOD	<LOD	18.57	2.35	27.29	8.38	171.72	72.48	16.58	1.46	89.16	3.08	117558.58	1712.03	225.66	5.89	7.27	1.64	1803.82	127.73	84.43	45.30	94.66	6.36	234.68	55.42
Domestic	8.52	27.95	23196.65	979.39	9.92	2.43	548.67	392.29	98031.76	4695.07	64.39	9.38	<LOD	<LOD	70.92	17.04	15393.05	341.61	13640.12	421.03	35.52	5.52	15687.77	3113.18	<LOD	<LOD	29.54	3.20	<LOD	<LOD	140.46	67.88	26.09	1.85	49.41	1.94	119147.60	1735.44	223.07	5.82	4.70	1.40	1492.02	110.78	56.06	36.54	69.43	4.96	405.08	95.66
Domestic	10.04	32.95	36102.09	1355.19	8.17	2.23	529.77	378.64	77527.08	3714.04	50.89	8.14	52.56	35.02	76.09	17.74	21001.65	461.34	23395.29	709.30	28.15	4.70	15661.30	3316.31	<LOD	<LOD	20.69	2.38	34.83	10.15	162.04	69.46	20.88	1.70	97.52	3.52	120937.67	1761.32	321.75	8.31	6.41	1.50	1857.78	132.55	97.78	47.66	78.97	5.30	208.10	49.15
Domestic	11.57	37.95	33563.24	1288.12	8.91	2.52	469.00	335.13	77309.52	3703.39	43.92	7.38	51.02	38.81	167.51	30.72	20787.99	456.18	23029.90	699.42	23.85	4.17	12994.33	2812.57	<LOD	<LOD	18.16	2.28	27.03	8.38	164.36	73.24	35.67	2.56	95.13	3.27	118128.04	1727.82	356.27	9.18	7.69	1.58	1962.67	139.57	95.99	47.09	112.40	7.38	217.22	51.30
Domestic	13.09	42.95	35414.83	1324.39	11.90	3.19	469.42	335.39	75297.12	3607.72	40.16	6.96	52.28	32.59	78.44	16.02	21550.66	472.25	24302.65	736.84	21.95	3.89	13179.54	2798.55	<LOD	<LOD	17.55	2.27	29.09	9.57	156.19	69.58	19.08	1.61	101.73	3.94	118268.56	1722.30	334.10	8.62	6.46	1.41	1956.63	139.40	95.72	44.39	82.40	5.44	222.49	52.54
Domestic	14.62	47.95	37271.12	1374.19	10.18	2.68	485.84	347.44	73134.95	3504.83	44.40	7.13	42.10	33.08	321.67	65.49	20460.70	449.16	24140.50	731.34	22.72	3.82	13269.03	2722.29	<LOD	<LOD	18.96	2.22	28.81	8.71	164.16	73.81	23.74	1.78	103.19	3.98	119472.08	1737.67	429.89	11.23	6.41	1.49	1970.13	137.31	99.03	47.13	116.47	7.49	209.84	49.55
Domestic	16.14	52.95	37746.84	1401.95	10.23	2.28	425.90	304.58	72193.84	3462.84	35.49	7.00	<LOD	<LOD	125.33	24.29	20669.71	453.74	23927.32	726.61	18.75	3.90	13741.64	2901.31	<LOD	<LOD	12.82	1.90	30.29	8.91	196.07	80.84	13.61	1.34	104.50	3.87	121704.23	1772.16	368.70	9.50	6.78	1.72	1963.79	136.30	105.03	57.77	94.27	5.98	238.85	56.40
Domestic	17.66	57.95	36670.87	1345.13	10.23	2.28	491.10	351.14	70797.58	3396.95	43.00	7.43	46.37	41.58	49.59	10.41	20733.81	454.69	23988.63	729.06	14.67	4.46	14588.38	3154.37	<LOD	<LOD	18.16	2.30	33.79	9.63	146.89	63.80	17.98	1.53	105.60	4.06	117091.07	1701.90	372.68	9.60	7.27	1.65	1967.63	135.25	101.19	54.89	77.64	5.33	237.42	56.07
Domestic	18.89	61.97	34864.48	1338.56	9.92	2.43	500.42	357.93	80126.93	3841.78	52.77	8.48	63.32	40.24	179.43	34.12	15261.54	451.11	22913.83	696.18	25.59	4.26	16888.01	3868.08	<LOD	<LOD	22.29	2.63	23.70	8.67	172.78	74.84	15.61	1.50	93.44	3.22	117799.42	1721.78	344.13	8.87	6.84	1.52	1850.40	132.27	102.40	50.99	151.22	9.05	204.14	48.21
Domestic	20.61	67.62	35162.92	1305.45	10.18	2.68	530.19	379.15	74964.45	3592.87	56.12	8.93	53.93	42.15	86.75	18.98	22094.88	484.61	21099.75	731.48	26.08	4.26	14886.14	3252.59	465.96	528.77	22.06	2.52	35.15	10.26	158.99	71.05	24.15	1.92	103.13	4.03	116380.01	1690.79	357.34	9.21	7.72	1.68	2038.82	142.36	93.54	48.40	78.53	5.41	199.86	47.19
Domestic	22.34	73.28	31702.68	1220.78	7.64	2.37	478.93	342.48	86206.65	4130.47	45.22	7.55	53.13	40.50	41.67	10.99	18782.26	414.25	16426.64	632.49	23.48	3.94	14256.62	2927.20	<LOD	<LOD	17.52	2.17	22.87	8.22	136.47	64.67	15.12	1.44	82.41	2.89	111942.04	1641.83	367.13	9.46	5.45	1.53	1714.03	119.69	83.25	48.13	73.40	5.21	284.79	67.31
Domestic	23.66	77.62	36244.02	1376.36	10.18	2.68	573.59	410.26	85459.93	4096.84	65.65	9.82	60.16	39.24	266.68	46.90	20251.62	446.25	24234.10	775.61	30.76	4.81	14019.50	2883.70	<LOD	<LOD	25.19	2.71	27.12	9.18	180.27	73.66	15.12	1.44	98.63	3.89	115315.07	1690.19	443.19	11.57	8.18	1.71	1806.93	127.01	106.09	58.39	109.63	7.35	201.78	47.66
Domestic	25.18	82.62	42915.47	1523.08	21.64	4.42	562.45	402.13	54011.82	2592.10	52.58	8.55	72.22	43.54	162.72	29.24	24540.50	535.75	29010.41	877.85	25.65	4.43	10493.98	2777.99	375.90	419.97	19.69	2.19	38.40	9.30	181.09	71.67	15.71	1.42	135.28	4.88	125338.68	1812.23	413.73	10.83	9.54	1.82	2290.14	157.06	138.06	65.22	102.62	6.97	187.26	44.23
Domestic	27.11	88.94	33348.27	1278.92	7.64	2.37	497.64	355.50	74978.76	3592.39	59.24	8.94	54.96	39.11	164.18	30.15	20239.48	444.58	20555.96	670.05	30.54	4.67	14494.69	3146.24	391.98	435.80	22.99	2.36	37.46	9.06	130.06	68.67	34.56	2.35	90.07	3.10	124820.38	1813.93	322.13	8.32	6.84	1.52	1974.25	136.87	99.55	49.66	102.63	6.87	201.10	47.49
Domestic	27.93	91.64	29479.26	1205.61	9.55	2.60	507.72	362.75	97272.20	4658.65	53.36	7.91	32.30	30.70	48.77	9.78	15770.77	351.06	17768.01	542.88	27.72	4.07	12157.17	4045.39	<LOD	<LOD	22.65	2.38	15.91	7.65	169.10	74.84	13.01	1.40	67.48	2.45	112319.17	1656.46	319.82	8.26	5.56	1.44	1541.17	113.49	65.70	39.65	65.29	4.74	235.86	55.70
Domestic	29.86	97.95	29386.76	1148.40	7.00	2.11	485.06	346.62	72947.76	3496.49	51.20	7.89	49.00	33.34	47.64	9.51	17308.70	382.55	18454.30	562.52	25.57	3.84	12479.00	2445.77	365.05	401.65	21.57	2.30	12.71	8.08	135.24	69.05	12.63	1.38																

Table A2-1. Willshire-21 particle size analysis table showing grain size as a percentage with depth.

Willshire-21 particle size data		>2000 µm	63-2000 µm	2-63 µm	<2 µm	32-64 mm	16-32 mm	8-16 mm	4-8 mm	2-4 mm	1-2 mm	0.5-1 mm	0.25-0.5 mm	0.125-0.25 mm	0.063-0.125 mm	0.032-0.063 mm	0.016-0.032 mm	0.008-0.016 mm	0.004-0.008 mm	0.002-0.004 mm	<0.002 mm	Method	
Depth (m)	Depth (ft)	% GRAVEL	% SAND	% SILT	% CLAY	% VERY COARSE GRAVEL	% COARSE GRAVEL	% MEDIUM GRAVEL	% FINE GRAVEL	% VERY FINE GRAVEL	% VERY COARSE SAND	% COARSE SAND	% MEDIUM SAND	% FINE SAND	% VERY FINE SAND	% VERY COARSE SILT	% COARSE SILT	% MEDIUM SILT	% FINE SILT	% VERY FINE SILT	% CLAY		
0.60	1.97		10.14	74.69	15.17						0.00	1.04	2.11	2.72	4.27	7.96	12.61	18.18	20.19	15.77	15.17	laser diffraction	
2.72	8.94		16.36	63.07	19.97						2.24	3.40	2.99	3.46	4.27	5.92	9.09	14.46	17.63	15.96	19.97	laser diffraction	
3.95	12.95		14.74	64.94	19.85						1.76	2.77	2.68	3.28	4.25	6.00	9.27	14.84	18.32	16.51	19.85	laser diffraction	
4.87	15.98		14.69	65.92	19.36						0.87	2.83	3.01	3.54	4.43	6.14	9.53	15.17	18.57	16.52	19.36	laser diffraction	
6.40	20.98		12.31	67.42	20.26						0.33	1.86	2.37	3.23	4.52	6.16	9.46	15.37	19.16	17.28	20.26	laser diffraction	
7.92	25.98		14.32	65.52	19.98						1.13	3.03	3.13	3.00	4.03	5.88	9.16	14.91	18.65	16.92	19.98	laser diffraction	
10.34	33.94		29.40	61.64	8.95						0.00	2.15	4.43	7.92	14.90	17.05	15.00	12.56	9.59	7.43	8.95	laser diffraction	
10.97	35.98		32.69	56.80	10.52						0.00	2.96	8.69	11.01	10.03	10.41	11.64	13.29	12.32	9.14	10.52	laser diffraction	
12.49	40.98		11.95	73.28	14.78						0.12	1.56	1.99	2.61	5.66	10.83	14.94	18.11	16.86	12.54	14.78	laser diffraction	
14.02	45.98		5.29	76.88	17.83						0.02	0.80	0.73	0.84	2.90	9.40	16.01	18.68	18.01	14.77	17.83	laser diffraction	
15.54	50.98		4.03	76.30	19.67						0.38	1.20	0.51	0.37	1.58	6.39	15.14	19.85	19.10	15.82	19.67	laser diffraction	
17.06	55.98		2.88	77.74	19.38						0.43	1.22	0.39	0.00	0.84	6.75	15.78	19.95	19.17	16.09	19.38	laser diffraction	
18.54	60.82		35.19	52.64	12.16						0.83	8.05	10.16	8.42	7.73	10.00	12.38	12.23	9.85	8.19	12.16	laser diffraction	
20.11	65.98		31.26	56.01	12.73						0.24	5.60	9.70	8.20	7.51	9.69	12.66	13.18	11.30	9.17	12.73	laser diffraction	
22.54	73.94		32.90	54.52	12.59						0.03	3.48	9.53	10.81	9.05	9.52	10.86	11.76	11.92	10.45	12.59	laser diffraction	
23.16	75.98		32.96	53.71	13.33						0.11	4.42	9.32	10.38	8.74	9.29	10.82	11.83	11.68	10.09	13.33	laser diffraction	
25.58	83.94		18.99	67.31	13.70						0.29	2.76	3.77	6.07	6.11	6.82	10.12	16.05	19.20	15.11	13.70	laser diffraction	
27.11	88.94		18.87	67.46	13.67						0.03	1.78	3.64	6.71	6.71	7.35	10.36	15.76	18.95	15.05	13.67	laser diffraction	
27.73	90.98		16.59	71.56	11.85						0.00	1.44	3.48	5.82	5.85	7.42	12.10	18.12	19.54	14.39	11.85	laser diffraction	
29.26	95.98		6.81	78.20	14.99						0.32	1.65	0.96	1.21	2.67	5.68	11.92	20.41	22.97	17.22	14.99	laser diffraction	
30.78	100.98	71.20	28.20	0.60		14.40	27.20	11.70	9.10	8.90	7.50	10.20	6.40	3.30	0.60					0.60		sieve	
32.55	106.80	66.50	31.80	1.70		6.90	27.00	12.70	9.50	10.30	11.50	9.40	4.00	4.80	2.10					1.70		sieve	
33.78	110.82	62.50	35.70	1.80			2.60	16.50	27.20	16.10	11.10	10.50	6.10	5.40	2.70					1.80		sieve	
35.50	116.48	21.40	74.20	4.30			4.70	5.00	6.10	5.60	7.90	21.20	20.10	16.30	8.70					4.30		sieve	
37.03	121.48	44.40	54.50	1.10			21.90	6.50	5.50	10.40	24.30	22.70	4.30	2.10	1.30					1.10		sieve	
38.45	126.15	54.30	44.70	1.00			5.10	12.70	15.90	20.50	25.20	13.50	3.30	1.50	1.20					1.00		sieve	
39.97	131.15	79.60	19.40	1.00		13.60	33.00	14.90	9.20	8.80	7.40	6.20	2.70	1.70	1.40					1.00		sieve	
42.25	138.61		29.99	54.48	15.53						0.34	6.14	7.36	6.90	9.26		11.37	11.50	11.83	10.59	9.19	15.53	laser diffraction
43.45	142.54		30.16	62.91	6.93						0.45	3.50	6.06	9.50	10.65		12.95	15.49	15.72	11.53	7.22	6.93	laser diffraction
44.60	146.31		31.45	57.00	11.55						0.06	3.29	7.42	10.64	10.05		10.81	11.91	12.98	11.93	9.37	11.55	laser diffraction
46.05	151.07		28.48	61.31	10.22						0.00	2.52	7.50	9.71	8.74	9.38		11.47	14.34	14.87	11.25	10.22	laser diffraction
47.57	156.07		29.07	61.11	9.82						0.11	3.56	7.32	9.46	8.62	9.27		11.45	14.39	14.87	11.14	9.82	laser diffraction
49.09	161.07		40.97	50.77	8.23						1.62	5.60	9.15	13.07	11.53		10.61	10.92	10.89	8.27	8.23	laser diffraction	
50.62	166.07		34.37	53.13	12.50						0.08	3.75	8.76	11.64	10.15		10.15	10.61	11.43	11.38	9.56	12.50	laser diffraction
52.14	171.07		21.06	67.91	11.03						0.00	0.89	4.43	7.24	8.49		10.40	12.84	16.88	16.64	11.15	11.03	laser diffraction
54.54	178.94		24.39	64.62	10.98						0.06	2.15	5.40	8.63	8.15		9.55	12.51	16.40	15.69	10.47	10.98	laser diffraction
55.16	180.98		33.47	55.73	10.80						0.05	3.42	8.51	11.23	10.24		10.50	11.26	12.50	12.16	9.31	10.80	laser diffraction
56.69	185.98		32.39	57.44	10.18						0.04	2.70	7.90	10.95	10.80		11.88	12.42	12.57	11.68	8.90	10.18	laser diffraction
58.21	190.98		33.02	56.19	10.79						0.20	3.61	7.30	11.22	10.68		11.31	11.86	12.25	11.67	9.10	10.79	laser diffraction
59.74	195.98		33.45	56.50	10.05						0.46	4.66	7.59	10.43	10.31		11.60	12.26	12.35	11.52	8.76	10.05	laser diffraction
61.26	200.98		31.51	59.86	8.63						0.00	1.45	5.05	9.33	15.69		17.67	14.08	11.55	9.46	7.10	8.63	laser diffraction
62.78	205.98		32.97	56.35	10.68						0.00	2.52	7.89	11.44	11.12		11.54	12.03	12.44	11.45	8.89	10.68	laser diffraction
64.31	210.98		33.78	56.10	10.13						0.21	2.91	7.69	11.62	11.35		11.87	12.13	12.29	11.14	8.68	10.13	laser diffraction
65.83	215.98		34.65	55.24	10.11						0.70	4.58	7.32	11.19	10.86		11.41	12.05	12.28	11.03	8.47	10.11	laser diffraction
67.36	220.98		29.37	60.59	10.04						0.19	3.75	7.37	9.51	8.55		9.43	11.70	14.38	14.25	10.83	10.04	laser diffraction
68.88	225.98		41.96	49.40	8.64						0.33	6.18	13.88	13.75	7.82		8.18	9.51	11.24	11.45	9.02	8.64	laser diffraction
70.55	231.48		2.79	80.80	16.17						0.96	1.17	0.33	0.00	0.33		2.63	11.30	23.26	25.19	18.41	16.17	laser diffraction
71.93	235.98		3.29	80.24	16.14						1.22	1.57	0.50	0.00	0.00		0.89	7.35	22.71	29.31	19.99	16.14	laser diffraction
73.90	242.46		2.07	87.56	10.37						0.00	0.00	0.00	0.01	2.06		11.64	22.59	24.91	17.64	10.79	laser diffraction	
74.98	245.98		53.57	43.93	2.50						0.00	0.00	1.01	16.77	35.80		26.55	8.37	4.06	2.84	2.11	2.50	laser diffraction
76.40	250.66		83.53	15.27	1.20						0.00	0.00	5.01	45.43	33.09		6.53	3.64	2.14	1.70	1.26	1.20	laser diffraction
78.02	255.98		77.65	20.42	1.93						0.00	0.00	2.83	34.43	40.39		8.50	3.93	3.30	2.63	2.05	1.93	laser diffraction
79.60	261.15	88.50	10.50	1.00		17.60	20.90	21.90	17.10	11.00	3.30	2.20	1.40	2.10	1.40					1.00		sieve	
81.12	266.15	89.10	10.30	0.60		17.20	24.40	19.60	18.90	8.90	3.80	2.30	1.30	1.30	1.50					0.60		sieve	
83.05	272.46		9.16	71.18	19.45						1.16	2.12	1.51	1.68	2.70		5.90	10.22	16.51	20.72	17.82	19.45	laser diffraction
84.12	275.98		3.70	83.11	13.19						0.00	0.72	0.30	0.01	2.67		11.22	15.91	19.64	20.95	15.38	13.19	laser diffraction
85.64	280.98		2.73	81.42	15.84						0.55	1.30	0.37	0.00	0.52		7.77	13.96	18.46	23.10	18.13	15.84	laser diffraction
87.17	285.98		5.00	75.59	18.71						2.03	2.09	0.51	0.00	0.37		2.02	8.52	19.16	25.17	20.72	18.71	laser diffraction
88.69	290.98		1.35	86.04	12.61						0.02	0.71	0.19	0.01	0.43		2.27	14.59	28.38	25.56	15.23	12.61	laser diffraction
90.22	295.98		22.47	65.20	12.33						0.26	3.99	5.53	5.70	6.99		10.48	13.13	15.68	14.82	11.09	12.33	laser diffraction
91.74	300.98	</																					

Table A2-2. Domestic particle size analysis table showing grain size as a percentage with depth.

Domestic particle size data		>2000 µm	63-2000 µm	2-63 µm	<2 µm	32-64 mm	16-32 mm	8-16 mm	4-8 mm	2-4 mm	1-2 mm	0.5-1 mm	0.25-0.5 mm	0.125-0.25 mm	0.063-0.125 mm	0.032-0.063 mm	0.016-0.032 mm	0.008-0.016 mm	0.004-0.008 mm	0.002-0.004 mm	<0.002 mm	Method	
Depth (m)	Depth (ft)	% GRAVEL	% SAND	% SILT	% CLAY	% VERY COARSE GRAVEL	% COARSE GRAVEL	% MEDIUM GRAVEL	% FINE GRAVEL	% VERY FINE GRAVEL	% VERY COARSE SAND	% COARSE SAND	% MEDIUM SAND	% FINE SAND	% VERY FINE SAND	% VERY COARSE SILT	% COARSE SILT	% MEDIUM SILT	% FINE SILT	% VERY FINE SILT	% CLAY		
1.20	3.94	0.00	14.53	63.56	21.44						1.71	2.67	2.76	3.29	4.10	5.91	8.68	14.14	17.80	17.03	21.44	laser diffraction	
2.82	9.27	0.00	16.03	61.69	21.49						2.42	2.86	2.33	3.38	5.04	6.76	8.53	13.15	16.86	16.40	21.49	laser diffraction	
4.25	13.94	0.00	14.27	62.26	22.75						2.26	2.93	2.50	2.93	3.65	5.16	7.91	13.73	17.99	17.46	22.75	laser diffraction	
5.57	18.28	0.00	10.17	64.90	24.39						1.76	2.10	1.76	2.09	2.46	4.00	7.66	14.15	19.74	24.39	19.74	24.39	laser diffraction
7.40	24.27	0.00	21.78	62.84	15.37						0.02	2.31	5.12	6.74	7.59	9.08	11.05	14.39	15.33	12.99	15.37	laser diffraction	
8.22	26.97	0.00	15.43	74.32	10.25						0.00	0.00	0.39	4.67	10.37	12.35	16.22	19.86	15.95	9.94	10.25	laser diffraction	
10.34	33.94	0.00	20.10	62.35	17.55						0.73	3.57	4.16	5.38	6.27	7.89	9.90	13.94	16.22	14.40	17.55	laser diffraction	
11.87	38.94	0.00	16.69	64.71	18.60						0.13	2.13	3.52	4.95	5.95	7.69	10.03	14.55	17.17	15.28	18.60	laser diffraction	
13.39	43.94	0.00	17.93	64.29	17.78						0.28	2.71	3.74	4.96	6.25	8.10	10.34	14.45	16.69	14.70	17.78	laser diffraction	
14.92	48.94	0.00	16.61	65.55	17.84						0.57	2.83	3.06	4.13	6.01	8.35	10.94	14.95	16.73	14.58	17.84	laser diffraction	
16.44	53.94	0.00	15.73	66.69	17.59						0.00	1.15	3.57	4.71	6.29	8.75	11.34	15.20	16.88	14.53	17.59	laser diffraction	
17.96	58.94	0.00	19.48	64.02	16.50						0.19	2.42	4.49	5.65	6.73	8.93	11.28	14.37	15.80	13.64	16.50	laser diffraction	
19.09	62.62	0.00	18.06	64.18	17.76						0.35	2.65	3.87	4.99	6.18	8.16	10.47	14.34	16.65	14.56	17.76	laser diffraction	
20.91	68.61	0.00	21.93	60.98	17.10						1.03	4.37	4.74	5.80	5.99	7.20	9.40	13.63	16.37	14.38	17.10	laser diffraction	
22.54	73.94	0.00	17.74	64.96	17.30						0.09	2.37	3.96	4.92	6.41	9.09	11.76	14.65	15.70	13.77	17.30	laser diffraction	
24.06	78.94	0.00	13.21	65.80	20.88						0.82	2.19	2.36	3.19	4.64	6.92	10.23	14.60	17.61	16.43	20.88	laser diffraction	
25.38	83.28	0.00	90.75	8.10	1.15						0.00	2.41	31.30	43.89	13.15	2.72	1.67	1.34	1.30	1.08	1.15	laser diffraction	
27.21	89.27	0.00	26.96	59.59	13.45						1.08	6.73	7.30	5.88	5.97	7.99	11.29	14.64	14.31	11.36	13.45	laser diffraction	
28.53	93.61	0.00	37.14	51.00	11.86						0.00	3.24	10.75	12.20	10.94	10.22	9.98	10.84	10.78	9.19	11.86	laser diffraction	
30.16	98.94	0.00	43.17	45.97	10.85						0.00	3.91	13.48	15.26	10.51	9.53	9.28	9.73	9.45	7.98	10.85	laser diffraction	
31.78	104.27	0.00	41.92	47.39	10.68						0.02	3.35	12.83	14.83	10.90	10.14	9.89	9.99	9.44	7.93	10.68	laser diffraction	
33.30	109.27	0.00	56.66	37.77	5.57						0.00	0.84	3.90	17.07	34.85	17.39	6.27	5.72	4.47	3.90	5.57	laser diffraction	
34.83	114.27	0.00	20.83	66.87	12.30						0.00	1.75	4.07	6.13	8.88	12.37	15.45	15.92	13.27	9.87	12.30	laser diffraction	
36.15	118.61	0.00	25.10	64.03	10.87						0.03	2.15	5.21	7.61	10.10	12.64	14.40	14.80	12.82	9.35	10.87	laser diffraction	
37.88	124.27	0.00	0.46	73.34	26.20						0.00	0.00	0.00	0.01	0.46	0.86	7.55	19.19	24.27	21.47	26.20	laser diffraction	
38.40	125.98	0.00	0.00	74.08	25.92						0.00	0.00	0.00	0.00	0.00	0.48	7.70	19.81	24.69	21.41	25.92	laser diffraction	
39.92	130.98	0.00	1.82	80.66	17.51						0.00	0.00	0.00	0.00	1.82	11.49	19.41	19.32	16.79	13.65	17.51	laser diffraction	
41.45	135.98	0.00	2.03	84.18	13.79						0.00	0.00	0.00	0.00	2.03	16.11	24.12	19.28	14.06	10.60	13.79	laser diffraction	
42.97	140.98	0.00	1.86	78.59	19.55						0.00	0.55	0.28	1.03	10.45	18.17	17.95	17.95	14.73	19.55	19.55	laser diffraction	
44.50	145.98	0.00	2.75	81.64	15.61						0.00	0.00	0.00	0.00	2.75	15.93	21.30	17.75	14.81	11.85	15.61	laser diffraction	
46.02	150.98	0.00	3.00	84.17	12.83						0.00	0.00	0.00	0.00	3.00	21.32	23.97	16.60	12.64	9.63	12.83	laser diffraction	
47.54	155.98	0.00	3.47	84.84	11.69						0.00	0.00	0.00	0.00	3.47	21.50	25.25	17.06	12.22	8.80	11.69	laser diffraction	
49.97	163.94	0.00	35.13	61.54	3.33						0.00	0.00	0.00	4.22	30.91	35.10	14.97	6.14	3.15	2.18	3.33	laser diffraction	
50.59	165.98	0.00	39.01	57.39	3.60						0.00	0.00	0.00	6.67	32.34	31.51	13.97	6.25	3.28	2.37	3.60	laser diffraction	
52.32	171.64	0.00	37.29	59.49	3.23						0.00	0.00	0.00	5.92	31.37	32.81	14.95	6.50	3.10	2.13	3.23	laser diffraction	
53.74	176.31	0.00	46.51	50.57	2.92						0.00	0.00	0.00	10.83	35.68	28.06	12.17	5.53	2.79	2.01	2.92	laser diffraction	
55.16	180.98	0.00	58.61	39.10	2.30						0.00	0.00	0.00	18.51	40.10	22.47	8.79	4.02	2.18	1.64	2.30	laser diffraction	
56.69	185.98	0.00	58.92	39.04	2.03						0.00	0.00	0.00	15.58	43.34	24.60	7.70	3.41	1.86	1.48	2.03	laser diffraction	
58.21	190.98	0.00	69.38	28.56	2.05						0.00	0.00	0.69	27.85	40.84	15.55	6.18	3.12	2.07	1.64	2.05	laser diffraction	
59.64	195.66	0.00	39.91	57.35	2.74						0.00	0.00	0.00	5.63	34.29	34.31	13.47	5.20	2.54	1.83	2.74	laser diffraction	
61.26	200.98	0.00	86.80	12.38	0.82						0.00	0.00	3.89	44.86	38.05	6.85	2.68	1.09	0.95	0.80	0.82	laser diffraction	
62.68	205.66	0.00	96.60	3.40							0.40	0.80	34.60	55.30	5.60								sieve
64.31	210.98	0.10	96.80	3.10						0.10	0.60	1.00	36.50	53.20	5.50								sieve
65.83	215.98	0.00	94.20	5.80							0.20	0.30	25.10	57.60	11.00								sieve
67.56	221.64	4.30	91.20	4.60				1.10	1.30	1.80	3.20	41.60	33.10	9.50	3.80								sieve
68.88	225.98	10.40	87.50	2.10			6.20	0.70	0.70	2.70	6.20	24.00	50.10	5.00	2.10								sieve
70.40	230.98	69.20	30.70	0.10			23.50	12.10	16.30	17.30	14.70	8.00	5.20	2.00	0.90								sieve
71.93	235.98	72.60	25.80	1.60		5.90	32.40	17.10	10.20	7.00	4.60	6.00	11.60	2.40	1.10								sieve
74.98	245.98	14.70	79.80	5.40			2.90	3.10	5.90	4.20	1.70	5.90	29.10	31.40	11.70								sieve
77.92	255.66	75.10	23.40	1.50			58.70	9.20	4.80	2.40	4.40	8.50	4.60	3.50	2.30								sieve
81.07	265.98	37.00	62.40	0.60			2.80	7.40	13.80	13.00	6.20	9.80	27.10	16.80	2.50								sieve
84.12	275.98	84.30	14.70	1.00		8.40	20.90	27.10	16.50	11.40	5.00	2.30	2.30	3.50	1.60								sieve
87.77	287.95	6.00	91.30	2.70				3.20	2.50	0.30	0.10	1.30	23.80	56.10	10.10								sieve
90.62	297.30	69.00	25.80	5.20		12.70	16.30	20.10	14.10	5.70	1.40	1.40	3.30	10.30	9.30								sieve
92.74	304.27		2.69	85.57	11.73						0.00	0.00	0.00	0.01	2.68		11.09	17.32	21.66	21.03	14.48	11.73	laser diffraction
94.26	309.27		11.69	82.45	5.86						0.00	0.00	0.00	0.02	11.68		33.04	23.88	12.59	7.76	5.17	5.86	laser diffraction
95.59	313.61		7.81	86.62	5.57						0.00	0.00	0.00	0.00	7.81		32.68	27.68	13.03	8.03	5.21	5.57	laser diffraction
96.21	315.66		9.33	86.16	4.51						0.00	0.00	0.00	0.02	9.31		35.23	27.93	12.15	6.79	4.06	4.51	laser diffraction
97.84	320.98	65.10	32.30	2.70		11.50	13.90	17.40	13.40	8.90	5.30	5.90	9.60	8.30	3.10								sieve
100.88	330.98	70.40	27.90	1.80			16.20	28.20	14.50	11.50	7.10	6.30	7.80	4.90	1.80								sieve
103.93	340.98	0.20	99.30	0.50							6.10	70.10	20.50										



